HHS Public Access

Author manuscript

Biomaterials. Author manuscript; available in PMC 2023 February 16.

Published in final edited form as:

Biomaterials. 2022 May ; 284: 121507. doi:10.1016/j.biomaterials.2022.121507.

Two-dimensional nanomaterials-added dynamism in 3D printing and bioprinting of biomedical platforms: Unique opportunities and challenges

Bipin Gaihre[a,b], **Maria Astudillo Potes**[a,b], **Vitalii Serdiuk**[a,b], **Maryam Tilton**[a,b], **Xifeng Liu**[a,b], **Lichun Lu**[a,b,*]

[a]Department of Physiology and Biomedical Engineering, Mayo Clinic, Rochester, MN, 55905, United States

[b]Department of Orthopedic Surgery, Mayo Clinic, Rochester, MN, 55905, United States

Abstract

The nanomaterials research spectrum has seen the continuous emergence of two-dimensional (2D) materials over the years. These highly anisotropic and ultrathin materials have found special attention in developing biomedical platforms for therapeutic applications, biosensing, drug delivery, and regenerative medicine. Three-dimensional (3D) printing and bioprinting technologies have emerged as promising tools in medical applications. The convergence of 2D nanomaterials with 3D printing has extended the application dynamics of available biomaterials to 3D printable inks and bioinks. Furthermore, the unique properties of 2D nanomaterials have imparted multifunctionalities to 3D printed constructs applicable to several biomedical applications. 2D nanomaterials such as graphene and its derivatives have long been the interest of researchers working in this area. Beyond graphene, a range of emerging 2D nanomaterials, such as layered silicates, black phosphorus, transition metal dichalcogenides, transition metal oxides, hexagonal boron nitride, and MXenes, are being explored for the multitude of biomedical applications. Better understandings on both the local and systemic toxicity of these materials have also emerged over the years. This review focuses on state-of-art 3D fabrication and biofabrication of biomedical platforms facilitated by 2D nanomaterials, with the comprehensive summary of studies focusing on the toxicity of these materials. We highlight the dynamism added by 2D nanomaterials in the printing process and the functionality of printed constructs.

Keywords

2D nanomaterials; 3D printing; 3D bioprinting; Tissue engineering; Toxicity; Therapeutic platforms

*Corresponding author. Mayo Clinic, Rochester, MN, 55905, United States. Lu.Lichun@mayo.edu (L. Lu).

Declaration of competing interest

The authors declare that they have no known competing financial interests or personal relationships that could have appeared to influence the work reported in this paper.

Appendix A. Supplementary data

Supplementary data to this article can be found online at https://doi.org/10.1016/j.biomaterials.2022.121507.

1. Introduction

1.1. Two-dimensional nanomaterials

The isolation of graphene layers in 2004 has led to unprecedented interests in two-dimensional (2D) nanomaterials [1,2]. A myriad of research endeavors demonstrating graphene's excellent electrical, mechanical, and thermal properties quickly stemmed in nanomaterials research arena [3,4]. The dimensionality of nanomaterials was identified as a critical parameter as the properties of 2D graphene were strikingly different from other forms of carbon [5,6]. Over the years, this insight on the dimensionality has led to the discovery of several other 2D nanomaterials with exotic properties compared to bulk materials [6,7]. Layered silicate nanomaterials, transition metal dichalcogenides, phosphorene, hexagonal boron nitride, graphitic carbon nitride, and transition metal oxides (Fig. 1) have emerged as promising 2D nanomaterials [6–8].

Optoelectronics, sensors, catalysis, supercapacitors, and batteries have been established as potential application prospects of these materials [9–13]. Additionally, their ultrathin structure has caught the attention of biomedical researchers to develop drug delivery, biosensing, theranostic, and gene sequencing platforms [14–17]. The high surface area to volume ratio of these materials has also inspired the research in developing nanocomposite scaffolds with enhanced mechanical and biological properties for tissue engineering and regenerative medicine (TERM) applications [18,19].

1.2. Three-dimensional printing

Three-dimensional (3D) printing, also referred to as additive manufacturing (AM), has emerged as a new paradigm driving significant innovations in biomaterials development and their applications for TERM. Stereolithography (SLA), powder bed fusion (PBF), digital light processing (DLP), and extrusion printing are some of the 3D printing techniques adapted widely in TERM [20]. The advantages offered by this technology, like design flexibility, architectural complexity, and high precision, have enabled the development of synthetic constructs resembling the anatomical structures [21,22]. Furthermore, enormous and rapid investment of resources on technological innovations has led to the advancement of available 3D printers that can accommodate the printing of biological factors and living cells at high-resolution [23–25]. This has not only enabled the development of disease and tissue models for therapeutic innovations but has also given a glimmer of hope towards the development of fully functional 3D organs [26–29].

1.3. 2D nanomaterials and 3D printing

The 3D printing of pristine 2D nanomaterials is challenging in several ways. For printing techniques based on photocuring of materials such as SLA or DLP, these materials inherently lack the chemical groups needed for such curing. Attempts have been made with the selective laser sintering (SLS) technique to 3D print the pristine 2D nanomaterials, especially graphene [30]. However, the outcome is limited by the lack of design flexibility and printing resolution. Several research endeavors have shown that modifying these 2D nanomaterials enable 3D printing either in aerogel or composite form. These studies have primarily utilized extrusion-based printing systems for such applications [31–34]. However,

the lack of relevant biological data with these systems, makes it difficult to affirm if these models would be suitable for biomedical applications as the property of 2D nanomaterials can vastly vary after the chemical modification [34]. Addition of pristine 2D nanomaterials to the biocompatible thermoplastics or hydrogels, thus, has been established as a viable avenue for the 3D printing of 2D nanomaterials for biomedical applications. Due to the ease of fabrication and lower associated costs, extrusion-based printing such as fused deposition modeling (FDM) and pneumatic extrusion systems are commonly used for TERM applications [35].

FDM systems require high temperature to enable the extrusion of fibers, making the technique almost impossible to incorporate the cells and biological factors during printing [36]. This essentially demands additional processing of the printed structures to generate the functionality for biological and biomedical applications. The incorporation of 2D nanomaterials into biocompatible thermoplastics has facilitated the development of multifunctional polymer composites. These composites have been applied for a range of biomedical developments, including scaffolds for tissue regeneration, platforms for photothermal and photodynamic therapies, and vehicles for drug delivery [37].

1.4. 2D nanomaterials and 3D bioprinting

Pneumatic extrusion printing systems that involve the pressure-induced extrusion of biomaterials from the needles and nozzles have garnered significant interest from researchers working on tissue engineering, *in-vitro* drug testing, and disease modeling [35]. The precision of printing combined with high printing resolution has enabled hydrogel-based system with controlled microstructure to better mimic the extracellular matrix (ECM) environment for tissue modeling and drug testing [27,38,39]. Furthermore, with the innovations in ink development, perfusion hydrogels have been developed, recapitulating the *in vivo* tissue environment for *in vitro* tissue and disease modeling [27,40]. Several parameters can affect the extrusion of biomaterials that could hinder the repeatability of the printing outcomes. In this respect, 2D nanomaterials, especially layered silicates, have received special attention in hydrogels' extrusion printing. The shear-thinning property of these materials, combined with their lower toxicity, has enabled the development of extrusion printable bioink that could incorporate cells with minimal-to-no adverse effects on their viability and functionality. The biocompatible and widely adopted polymers such as gelatin methacrylate (GelMA) have been shown to become printable with high printing fidelity when combined with such materials [41–43].

Additionally, emerging reports on the applicability of 2D nanomaterials, other than layered silicates, for bioprinting with cells have unlocked advanced and exciting avenues to use less explored 2D nanomaterials for such applications. Recently, 3D bioprinting of graphene oxide (GO) hydrogels with mesenchymal stem cells (MSC) was reported. Such constructs preserved the long-term viability of MSC, with GO having a direct effect on the osteogenic differentiation of bioprinted MSC [44].

1.5. Introductory synopsis

At the outset, this review emphasizes on biomedical applications of 3D printing and bioprinting, and the recent advancements in this area leveraged by unique properties of emerging 2D nanomaterials at disposal. We present a comprehensive overview of several 2D nanomaterials-based 3D printed platforms developed for tissue engineering, tumor therapies, and drug delivery. We also outline the current advancements in 3D bioprinting of hydrogels with 2D nanomaterials and multifunctionalities imparted by these materials towards developing functional constructs. Finally, we present a critical summary of toxicity aspects of 2D nanomaterials (Table 1).

2. Carbon-based 2D nanomaterials

Nanomaterials based on carbon, such as carbon nanotubes (CNTs), were popular choices because of their excellent conductive properties for several applications [45]. Though CNTs are still used in divergent nanomaterials research areas, the emergence of a 2D form of carbon known as graphene has dominated this space since its discovery. The properties such as higher specific surface area, ease of functionalization, and lower production cost make graphene unique from CNTs while maintaining properties such as excellent mechanical strength, electrical conductivity, and biocompatibility like CNTs [1,45]. Structurally, graphene is a layer of sp2-bonded carbon atoms arranged in a hexagonal lattice and can be referred to as one atomic layer of graphite. The family of graphene 2D nanomaterials comprises graphene, GO, and reduced GO (rGO). In general, these nanomaterials have been considered safe for biological applications, dependent on the concentration and size of the particles (Table 1). The modified form of these nanomaterials such as PEG functionalized rGO have shown some level of local toxicity (Supplementary Table 1).

2.1. Graphene

Graphene, an exciting 2D material, has found its applications in different frontiers of biomedical applications after its discovery back in 2004 [1,46]. Given significant progress in developing graphene-based materials, 3D printing of pure graphene without chemical modification or without usage of binders is challenging, especially with direct ink writing. Other AM techniques, such as SLS, have been successful only for printing graphene in the composite form.

Sha et al. attempted to 3D print the pristine graphene foams. As shown in Fig. 2A, it involved CO_2 laser sintering of manually fed powder of nickel and sucrose. Sucrose acted as a solid carbon source for graphene and nickel as catalyst and substrate for graphene growth. After 20 cycles of laser irradiation, the resulting twenty-layered nickel-graphene was treated with ferric chloride ($FeCl_3$) solution to etch out the nickel. The laser path guided the structural design of pristine graphene foam [30]. This technique presented a method to 3D print bulk graphene structures which lacked precisely designed complex and rational topologies typically expected of AM modalities.

The direct ink writing or extrusion printing of graphene with polymeric binders is a well-established technique to develop the constructs by preserving the conductive properties of

graphene for biomedical applications. Jakus et al. applied polylactide-co-glycolide (PLG) to print elastomeric graphene composites with neurogenic potential. Graphene (3–8 atomic layers thick) was combined with PLG at 60%, 40%, and 20% (volume %) for 3D printing. The extrusion printing of graphene-PLG was performed at room temperature without a melting the polymer (Fig. 2B: a). The randomly dispersed graphene flakes in PLG solution were highly aligned and oriented along the fiber surface after printing, as shown in Fig. 2B: b-e. Due to the elastomeric nature of PLG, the printed structure was flexible and moldable (Fig. 2B: f). The electrical conductivity of the printed scaffolds with 60% and 40% graphene was close to 600 S/m compared to approximately 100 S/m for 20% samples.

Furthermore, the conductivity was higher for the constructs printed with a lower diameter extrusion nozzle which showed the importance of graphene alignment for effective conductivity. The scaffolds with such a high concentration of graphene appeared to support the viability and proliferation of MSC.

Additionally, even in the absence of neuro-differentiation supplements, MSC were observed to develop axonal elongation on the 60% graphene scaffolds (Fig. 2B: g-i). The upregulation of neurogenic factors on these scaffolds further confirmed the differentiation activities [31]. Thus, graphene ink applications were further expanded for bone tissue regeneration by combining it with hydroxyapatite (HA) microparticles. The 35% dry powder of HA was combined with 35% graphene flakes and 30% PLG to formulate a composite ink for extrusion printing. Though the addition of HA was observed to lower the electrical conductivity of scaffolds, the neuronal differentiation of MSC was not affected. Additionally, upregulation of osteogenic markers was observed [47].

The facile extrusion printing method established for polycaprolactone (PCL) makes it an attractive polymer choice to develop 3D printed scaffolds for bone tissue engineering. The addition of graphene to such scaffolds has been shown to impart the scaffolds with added benefits such as electrical conductivity, improved mechanical properties, and enhanced cell responses on the scaffolds [48–50]. The *in vivo* implantation of 3D printed PCL-graphene scaffolds in rat calvarium defects followed by electrical stimulation at 10 μA for 5 min, twice a week, resulted in higher tissue formation at the defect site. A clear difference in mineralized tissue was not observed in groups with electrical stimulation. However, improved osteoblast remodeling activities were apparent, as indicated by the upregulation of RANKL/OPG markers [50].

2.2. Graphene oxide

The increased hydrophilicity of graphene oxide (GO) compared to graphene makes it more attractive for biomedical applications. The caveat, however, is a significant reduction in electrical conductivity and mechanical strength [51]. Unlike applications in nanoelectronics and sensors, the electrical conductivity of GO has been demonstrated to instill sufficient stimulatory behavior for biological activities. The possibility of facile chemical modification of GO and eventual combination with polymers has enabled the achievement of sufficient mechanical strength of GO in composite formulations [52,53].

Like graphene, the 3D printing of GO is mostly accomplished with direct ink writing. The development of ultralight graphene aerogels is of particular interest due to their superior mechanical properties, high surface area, and extraordinary electrical and thermal conductivity [33]. The development of graphene aerogel microlattices has been accomplished using 3D printing technology [32,33]. The biggest challenge, similar to that for direct ink writing of graphene, is the unsuitable rheological properties of GO aqueous suspension without incorporating additives.

The higher concentration of GO in the alkaline suspension can induce its gelation [54]. It can also undergo gelation with sol-gel polymerization of resorcinol and formaldehyde using sodium carbonate as a catalyst [55]. Zhu et al. applied these techniques of forming GO aerogel to 3D print the aerogel microlattices (Fig. 3A). Their observation showed that adding hydrophilic silica powders to a high concentration (20 mg/ml and 40 mg/ml) GO suspension can superiorly improve the rheological properties of suspension, making it suitable for extrusion printing (Fig. 3B). The addition of 20% and 10% silica to 20 mg/ml and 40 mg/ml GO suspension increased the elastic modulus and yield stress by order of magnitude and over an order of magnitude, respectively (Fig. 3B) [33].

Jian et al. showed that calcium chloride could induce the ionic gelation of GO and impart shear thinning behavior suitable for extrusion printing. Compared to the earlier reports, this method of printing GO aerogel microlattices appears to be more facile, superficial, and bio-friendly [32] (Fig. 3C). To obtain microfibrous scaffolds, GO gel with calcium chloride can also be subjected to microfluidic printing [56]. The studies discussed here utilized one or the other gelling agents as additives for extrusion printing of graphene.

In a different approach, studies have focused on the concentration-dependent thickening of aqueous GO colloids [57,58]. Beyond critical concentration in aqueous colloid solution, GO can undergo liquid crystalline phase transition making the rheological properties suitable for extrusion printing Interestingly, until recently, 3D printed GO scaffolds, mostly in pristine form, have not been explored much for their biological functionalities. Lu et al. utilized ferric (Fe) ion-induced gelation of concentrated GO suspension for the extrusion printing of GO hydrogels, intended for tissue engineering applications. Fe ions were observed to improve the rheological properties and printing fidelity in a concentration-dependent manner. The stability of printed structure supported the post-lyophilization process to obtain porous struts, which were observed to promote hepatic cell attachment on the printed structure [59].

The applications of GO as a filler phase in polymeric matrices or as an additive for bioceramics have attracted significant attention for the development of nanocomposite scaffolds for tissue engineering and antibacterial treatment [60–62]. The commonly used 3D printing technologies such as microextrusion or stereolithography have been applied to develop GO-based 3D printed composite scaffolds [63–65]. 3D printed polymer scaffolds with macroporous morphology often compromise the mechanical properties of the bulk polymer. Incorporation of microporous morphologies into the 3D printed polymer scaffold’s design alters the mechanical properties of the bulk polymer. The inclusion of GO to these polymers can facilitate additional degree of freedom to further control these mechanical

properties [66,67]. Furthermore, 3D printed scaffolds fabricated for bone tissue engineering have superior osteogenic behavior because of GO incorporation [68,69]. Recent studies have shown that GO incorporation can also upregulate chondrogenic differentiation of MSC on 3D printed hydrogels [63,64, 70]. The 3D organization of GO facilitated by the printing process has also induced antibacterial properties to the PCL scaffolds, especially against *S. epidermis* and *E. coli* [71]. Furthermore, the reactive charged groups of GO make it a favorable bioactive coating moiety that can modulate the cellular responses on the surface of 3D printed scaffolds [72,73].

Owing to the lower conductivity of GO compared to graphene, its incorporation method and design of 3D printed scaffolds appear to be vital to achieving the maximum beneficial effects of GO for nerve regeneration. Qian et al. utilized 3D printing technology to perform layer-by-layer casting of GO-PCL and develop the conduits for peripheral nerve regeneration. Their results showed that loading GO to conduits enables Schwann cells to function better for nerve regeneration, including recovery of motor and electrophysiology activities [74]. By using PCL as a template, Zhang et al. showed that GO-coated 3D printed structures could not significantly improve the neurogenic activities of PC-12 cells. However, the anisotropy in the design of printed scaffolds, could elicit better neurite extension compared to isotropic architectures [73] (Fig. 3D).

With the rapid emergence of 3D bioprinting, a subset of 3D printing technology where cells and bioactive factors are incorporated into a printable ink, GO has found recent attention as an additive to improve the printing fidelity, and overall biological activity of 3D printed bioink [63,64,75]. Zhang et al. reported that the addition of GO to alginate/-gelatin bioink increased the viscosity, improved shear-thinning behavior, and promoted shear recovery of the bioink resulting in a high printing fidelity with GO. Bioprinted constructs with GO supported long-term (up to 42 days) viability of encapsulated human MSC while promoting their proliferation and spreading within the constructs (Fig. 4A–B). Furthermore, bioprinted cell-laden constructs showed a progressive increase in mineralization under osteogenic medium maintained in a bone bioreactor with higher mineral volume observed on samples with GO [44] (Fig. 4C–E).

2.3. Reduced graphene oxide

The interruption of graphitic sp^2 by oxygen-containing bonds in GO results in loss of charge transport capacity of GO [76]. Subsequently, GO is often applied in reduced form as rGO to restore the electrical conductivity of graphene sheets [76,77]. rGo has been pivotal for the development of several biosensors, photodynamic and photothermal therapy applications, and functional nerve guide conduits [78–84].

3D printed form of rGO has been developed mostly from the 3D printed GO due to the ease of fabrication and the eventual chemical or thermal reduction process [56,85]. For example, 3D printed GO aerogel microlattices can be treated with hydroiodic acid for the chemical reduction to produce rGO microlattices [32].

The application of 3D printing techniques to create microfibrous scaffolds has enabled the continuous distribution of rGO with the eventual benefit of efficient transmission of

electrical signals for nerve regeneration applications. In a recent study, Wang et al. utilized near-field electrostatic printing, a technique that combines electrostatic spinning and 3D printing, to develop microfiber patterns (15–148 μm) of GO incorporated poly (L-lactic acid-*co*-caprolactone) (PLCL). Individual microfibers of PLCL primed with cationic groups underwent electrostatic interaction with anionic GO, which were eventually patterned into 3D mesh before subjecting to L-ascorbic acid induced reduction of GO to rGO (Fig. 5A). Such microfiber patterns with uniform rGO coating showed a maximum electrical conductivity up to 0.95 Scm^{-1}. As a result, under electrical stimulation, magnitude-dependent neurite outgrowth of PC-12 cells was observed. The outgrowth was independent of the direction of electrical stimulation, and rather the neurites were found to be tightly distributed along the microfiber orientation. Several other patterns of microfibers, such as the spiderweb-like patterns were printed, and similar fibrillary orientation of neurite outgrowth was observed along the radial and axial directions. The fibrillary orientation of neurite outgrowth was not affected when the patterns were rolled into a tube. The neurite outgrowth of 1.96 mm and 2.5 mm was observed for PC-12 cells and mouse neurons along the longitudinal direction of tubes, respectively [82] (Fig. 5B–C).

In another recent study, Fang et al. developed rGO-mesoporous silica composite termed nanocookie (NC) incorporated into a commercially available resin to 3D print the nerve conduits responsive to magnetoelectric stimulation. Using digital light processing (DLP), the design rationale of this study enabled the exposure of NCs on the surface of the conduits for efficient magnetoelectric conversion and consequent release of neuronal growth factors to modulate PC-12 cell activities [81]. Like GO, rGO has also been found to improve the osteogenic properties of 3D printed polymeric and ceramics scaffolds [86,87]. There is no clear deduction on the actual mechanism of rGO promoting the osteogenesis of 3D printed scaffolds and has been generally assigned to a combination of various outcomes such as the increase in surface roughness and stiffness.

3. Layered silicate clays

Clays used in biomedical applications are layered silicate materials mostly belonging to smectites [37]. These materials, especially Laponite and Montmorillonite, are popular due to their biodegradability, mostly degrading to non-toxic components and better biocompatibility than other 2D nanomaterials at comparable concentrations (Table 1). The net negative surface charge makes them attractive for localized and controlled delivery of drugs and growth factors for tissue engineering applications [24,88,89]. The weak surface charges enable the facile delamination of individual layers, facilitating clays' nanoscale interaction with other molecules. Furthermore, due to their hydrophilic surface chemistry, these materials impart unique rheological properties to the aqueous polymer solutions making them attractive fillers for the extrusion-based 3D printing of hydrogels [90–92].

3.1. Laponite

Laponite consists of lithium and magnesium oxide layers sandwiched between two silicate layers (Fig. 6A). It has been known for its gel-forming ability in water resulting from ionic interactions between the anionic surface and cationic edges of clay particles assembled

into a house-of-cards structure (Fig. 6A). It has been explored significantly as an additive for 3D printing of mechanically robust hydrogels as it offers the shear-thinning properties to facilitate extrusion printing with high shape fidelity [42,93–95]. Furthermore, its yield stress properties have unlocked exciting directions in additive manufacturing such as direct ink writing of self-supporting hydrogels on air in the form of aerogels [96], support-bath assisted 3D bioprinting of cell-laden hydrogels [97], and clinically relevant intracorporeal 3D printing [98]. The ionically interacted Laponite with charged polymers such as kappa-Carrageenan included within the covalently crosslinked GelMa has resulted in several studies on 3D printing for tissue engineering applications [90, 99–102]. Such combination could generate 3D printed structures with high structural stability and shape fidelity that can ultimately facilitate the development of complex anatomical structures (Fig. 6B) [100].

Liang et al. applied Laponite to coaxially print micro-tubular hydrogel structures of GelMa and N-acryloyl glycinamide (NAGA) for potential application as tubular tissue grafts. The interpenetration of Laponite to the polymer network allowed shear thinning of the hydrogels that eventually facilitated scalable manufacturing of the tubes. Hydrogel microtubes possessed swelling stability, high toughness, superior stretchability, excellent perfusion, and controllable permeation. Additionally, the microtubes were biocompatible and supported accelerated endothelialization [103] (Fig. 6C–D).

Due to the presence of bioactive elements, Laponite has also found significant interest in the development of 3D printed bone scaffolds [104–107]. Zhai et al. used it to empower the extrusion printing of polyethylene glycol (PEG) hydrogels. Employing a two-channel printing process, they successfully fabricated layer-by-layer constructs comprising of PEG-clay composite and cell-laden hyaluronic acid. This layer-by-layer deposition of cells elicited significant improvement in osteoblast response, explicitly relating to distribution along the constructs, with enhanced viability and osteogenic differentiation compared to static cell seeding post-printing of hydrogels. This excellent osteogenic behavior was further reflected in *in vivo* studies where an enhanced bone formation was observed with cell-laden PEG-clay constructs in the tibia repair model (Fig. 7A) [108].

Among the several classes of 2D nanomaterials discussed in this article, clays have found significant interest in 3D bioprinting applications. Their excellent cytocompatibility (Table 1 and Supplementary Table 1) coupled with the ability to impart the shear thinning behavior to cell-loaded pre-hydrogel solutions has inspired researchers to utilize these materials for extrusion bioprinting applications [101,104,106, 109]. The cells mixed with pre-hydrogel solution can be subjected to shear stress through small diameter needles or nozzles during the pneumatic extrusion. Due to the shear thinning of hydrogels during extrusion facilitated by the clay particles, lower shear stress is exerted on the cells that help to improve the cell viability after extrusion. Furthermore, for naturally sourced polymers such as GelMa, which lack sufficient mechanical stiffness, clay incorporation has been found to improve the hydrogel strength and post-crosslinking stability of the printed GelMa structure. One of the critical parameters in 3D bioprinting is the UV exposure time, as prolonged exposure time for polymer crosslinking can negatively affect the bioprinted cells. For polymers like alginate that can undergo ionic crosslinking with divalent ions, bioprinting cell-laden constructs with long-term stability might not be the problem [110]. However,

for photocrosslinkable polymers, the optimization of crosslinking time is pivotal to elicit minimal adverse effects on cells while ensuring complete polymer crosslinking to achieve a stable cell-laden construct. The addition of clays to these polymers can provide the added benefit for such needs. The presence of charged clay particles enables ionic entanglement with the oppositely charged polymers, which can be advantageous to improve the long-term stability of bioprinted cell-laden hydrogels. One of such strategies developed is shown in Fig. 7B, where Laponite clays are entangled with the electrostatically coiled structure of kappa-Carrageenan and GelMa chains, thereby creating a secondary ionic crosslinking mechanism that improved the viscoelasticity and printability of the bioink [99]. This bioink, termed nanoengineered ionic-covalent entanglement (NICE), has been shown to support the long-term viability of the bioprinted cells with excellent osteogenic behavior suitable for bone tissue regeneration [101].

3.2. Montmorillonite

Montmorillonite (MMT) consists of an aluminum oxide layer sandwiched between two silicate layers. Comparatively, MMT clays have found less interest in 3D printing and especially bioprinting applications. There are sparse reports of MMT clays used for FDM and SLA printing of polymers [111–113]. The use of MMT for the extrusion printing of hydrogels is especially under-researched. We strived to utilize acrylated-MMT to facilitate the extrusion printing of oligo[poly (ethylene glycol) fumarate] (OPF) hydrogels [114]. We observed that, in addition to supporting high fidelity printing of OPF, MMT also enhanced the osteogenic differentiation of bioprinted pre-osteoblasts. Additionally, MMT has also been reported to support the 3D bioprinting of alginate hydrogels [115]. With emerging reports on focused on MMT incorporated hydrogels supporting an excellent cell behavior [116], the interest is expected to rise for the MMT-facilitated 3D printing and bioprinting of hydrogels.

4. Black phosphorus

Like graphene, black phosphorus (BP) is metal-free and has stacked layers of phosphorus that can be exfoliated into nanosheets or nanoparticles, quantum dots, and nanoribbons [117–119]. Nano-BP consists of six phosphorus atoms arranged in a unique puckered ortho-rhombic structure. It has been shown to generate singlet oxygen species with visible light irradiation and heat with near-infrared (NIR) irradiation [120]. Consequently, there has been a rapid surge in research interests of BP in the current paradigm of biomedical applications, including photodynamic therapy and photothermal therapy of tumors, in addition to biosensing and bioimaging [121–127]. Furthermore, its biocompatibility and biodegradability, have also found an elevated interest as a biomaterial for tissue repair [128]. The level of toxicity imposed by these nanomaterials is largely dependent on the size, concentration, and duration of exposure (Table 1). The major degradation products of BP are phosphates and phosphate ions, which do not pose any safety concerns to the human body. Given the role of phosphorus and phosphates in the development of bone, researchers have focused on developing BP-incorporated 3D printed scaffolds primarily for bone regeneration with an inherent photothermal or photodynamic therapy potential [72,129–131].

Yang et al. developed BP nanosheets coated 3D-printed bioglass (BG) as BP-BG 3D scaffold. These scaffolds were shown to generate photothermal ablation toward osteosarcoma and enhance subsequent bone regeneration. The hypothesized mechanism is shown in Fig. 8A. The biodegradation of BP nanosheets was expected to release a large quantity of phosphate ($PO4^3$) ions. The availability of calcium ions in the body fluid was further expected to trigger the biomineralization at the implantation site, eventually improving bone regeneration. They demonstrated these photothermal and bone formation activities with 3D printed BP-BG scaffolds using an osteosarcoma model in mice and a calvarium defect model in rats [129].

A multifunctional 3-D printed PLGA structure incorporated with BPNs, β-tricalcium phosphate (β-TCP), doxorubicin (DOX), and bone morphogenic protein-2-like osteogenic peptide (P24) was developed by Wang et al. using the microextrusion technique. The photothermal and chemical ablation of the tumors was achieved with BPNs and DOX. Incorporating BPNs within the PLGA matrix enabled prolonged photothermal effects lasting up to 4 weeks and modulated the release of DOX and P24 from the scaffolds. The implantation of scaffolds with BPN and DOX and subsequent NIR irradiation at the tumor site in mice resulted in significantly reduced tumor volume just after 4 days. However, the recurrence of the tumor was not prevented by scaffolds with only BPN, which suggested that tumor ablation due to BPN induced photothermal activity may not be sufficient to prevent the continuous re-growth of the tumor. In contrast, the combined effects of BPN and DOX prevented tumor recurrence. Excellent osteogenic responses further complemented the anti-cancer potential of these scaffolds due to the presence of β-TCP and P24. The scaffolds with β-TCP and P24 or all four components showed significant healing of calvarial bone defects compared to other groups (Fig. 8B) [130].

5. Transition metal dichalcogenides

Transition metal dichalcogenides (TMDs) are a class of 2D nanomaterials with a general structure of MX_2, where a monolayer of transition metal atom M (Ti, V, Mo, W) is sandwiched between two layers of chalcogen atom X (S, Se, Te) (Fig. 9A) [132]. These 2D nanomaterials are known in optoelectronics for their unique properties, such as direct bandgap, strong photoluminescence, and large exciton binding energy [133]. Furthermore, their catalytic properties, optical absorption, and high wear resistance make them an exciting biomaterial for biosensors, bioimaging, and photothermal and photodynamic therapy [134,135]. A better understanding of the biological properties of these nanomaterials has evolved over time. Similar to other 2D nanomaterials, the toxicity effects are largely dependent on the concentration (Table 1). Cell responsive modifications have been shown to mitigate the toxic effects of these nanomaterials at higher concentrations (Supplementary Table 1).

Transition metals in disulfide form such as molybdenum disulfide (MoS_2), tungsten disulfide (WS_2), and titanium disulfide (TiS_2) have found attention in biomedical applications [136]. Mainly, MoS_2 and WS_2 have been studied for 3D printing of scaffolds with tumor therapeutic and bone regenerative potentials [137–139].

MoS_2 nanosheets have been used mostly to create a coating on the surface of 3D printed osteogenic scaffolds to impart those scaffolds with dual bone regeneration and tumor ablation [137,138]. Wang et al. developed akermanite (AKT) based 3D printed scaffolds combined with MoS_2. To utilize the excellent NIR absorbance property of MoS_2 nanosheets for photothermal tumor therapy, they employed hydrothermal treatment for the *in-situ* growth of MoS_2 nanosheets on the surface of such scaffolds. The AKT-MoS_2 scaffolds displayed photothermal behavior with temperature rise to 115 °C when irradiated at 0.5 W cm^{-2} (Fig. 9B), which induced *in vitro* tumor ablation against bone tumor cells and breast cancer cells. As shown in Fig. 9A, this photothermal behavior was further observed i*n vivo*, with the temperature of the tumor site reaching up to 50 °C under irradiation without affecting the temperature of the surrounding healthy tissues. The rapid rise of the temperature resulted in the lower tumor volume on the functionalized scaffold group with irradiation compared to non-functionalized scaffolds (Fig. 9B). The photothermal behavior at the tumor site due to MoS_2 functionalization was shown to have non-significant effects on the excellent osteogenic capabilities of AKT biomaterials. The implantation of scaffolds demonstrated this on the femoral head of rabbits, where the new bone formation was not affected by the photothermal behavior at the bone implantation site [138].

WS_2 nanotubes and nanosheets are found to be excellent physical reinforcing agents for biodegradable polymers [140]. Chen et al. employed the chlorophyll pigment-assisted exfoliation of WS_2 to improve its dispersion in the polymer solutions (Fig. 10A). They demonstrated that adding such nanosheets at 5% (w/w) to PCL-calcium silicate composite could improve the compressive strength and modulus of 3D printed composite scaffolds by 300% and 450%, respectively. Furthermore, WS_2 incorporated composite scaffolds showed higher collagen I absorption to the surface, facilitating early-stage MSC attachment and improving osteogenic differentiation than the scaffolds without WS_2. The excellent *in vitro* responses were further replicated in *in vivo* bone formation where WS_2-incorporated 3D printed scaffolds were observed to have higher bone formation in rabbit femoral defects than other groups without WS_2 (Fig. 10B–C) [139].

6. Transition metal oxides

Transition metal oxides (TMOs) are long-studied nanomaterials due to their wide range of electronic, chemical, mechanical, and thermoelectric properties [141]. While TMOs such as molybdenum trioxide (MoO_3), tungsten trioxide (WO_3), gallium (III) trioxide (Ga_2O_3), and vanadium pentoxide (V_2O_5) possess intrinsic layered 2D atomic structure, TMOs more relevant to biomedical applications lack this property. For instance, titanium oxide (TiO_2), manganese oxide (MnO_2), and cobalt oxide (CoO) all require further processing to obtain the 2D form of these nanomaterials [142]. Several techniques, such as gas and liquid phase exfoliation, have been adapted for the synthesis of 2D TMOs. While the gas phase process is more complex and challenging, simple bottom-up synthesis such as liquid-phase exfoliation has been successfully demonstrated to synthesize TiO_2, MnO_2, zirconium, and aluminum oxides [143]. The biological applications of TMOs such as MnO_2 and TiO_2 span bioimaging, drug delivery, biosensing, and tumor therapy [144]. With potential acute toxicity imposed by these nanomaterials, special precautions should be taken while considering these nanomaterials for biomedical applications (Table 1).

MnO_2 nanosheets consist of interlayer cations between monolayers composed of metal oxide octahedral units. Due to convenient functionalization routes and Mn ion sensitivity to magnetic signals, MnO_2 has found special attention for targeted magnetic resonance imaging (MRI) of tumors [145]. These properties, combined with its ability to modulate the hypoxic tumor microenvironment by attenuating the expression of hypoxia-inducible factor-1α, have made it an attractive 2D material for developing nano theranostics platforms [146,147]. The glutathione-mediated degradation of MnO_2 has inspired its investigation as potential drug carriers with high target specificity and efficacy [148]. The use of 3D printing technologies to develop MnO_2 based platforms has not been extended to biomedical applications though it has been explored for the development of energy storage devices and micro-batteries [149,150].

TiO_2 is another TMO that has found several applications in the biomedical field [151]. Structurally, TiO_2 possesses a wide-bandgap that provides it with a photo-absorption property at the UV range. It has found interest in developing UV light-based photodynamic therapy platforms for tumor therapy [152]. The challenges associated with the clinical application of UV light-based systems have further inspired the modification of TiO_2 to shift the absorption band to NIR/visible range or make it responsive to sound signals [152–154]. TiO_2 has been used as the UV-filter component of 3D printable resin for high-resolution printing of polymers using continuous digital light processing [155, 156]. It has also been used as an additive to 3D printable polymers or as a coating material to improve the surface properties of printed scaffolds [157,158]. The addition of TiO_2 was shown to improve the overall mechanical and biological properties of the 3D printed scaffolds for bone tissue engineering [157].

7. Hexagonal boron nitride and graphitic carbon nitride

Hexagonal boron nitride (hBNs), due to their excellent thermal properties and electrical insulating properties, are primarily 3D printed with resins and thermoplastics to develop well-designed composites for applications in electronics and aerospace [159,160]. Structurally, the hBN layer consists of alternating boron and nitrogen atoms (Fig. 11 A). It has been studied for drug delivery, biosensing, and imaging to some extent [161]. TERM application of these materials, including 3D printing, is yet to be explored adequately. Guiney et al. showed hBN could be extrusion printed with PLGA to develop nanocomposites with high thermal conductivity [162]. With a higher concentration of hBN, it was demonstrated that some complex structures with excellent structural stability could be printed (Fig. 11B).

Interestingly, hBN was observed to increase the viability, attachment, and proliferation of MSC on the PLGA scaffolds (Fig. 11C). This study laid the foundation for a few recent studies where researchers aimed to 3D print hBN scaffolds for bone tissue engineering applications [163,164]. The mineralization of pre-osteoblasts grown on the 3D printed scaffolds was demonstrated to increase due to hBN functionalization [164].

The application of graphitic carbon nitride (gCN) like that of hBN is slowly emerging over the past few years in the biomedical field. Structurally, gCN (accurately: g-C_3N_4) is a

polymeric material composed of tris-triazine-based patterns with a carbon to nitrogen ratio of 3:4 and a small amount of hydrogen. It has visible light absorption and photocatalytic properties and has found biomedical applications in diagnostic imaging, therapeutic platforms, biosensors, and antibacterial applications. For tissue engineering applications, although previous studies have demonstrated the biocompatibility of bulk gCN, lack of aqueous dissolution and biodegradation can create challenges for further applications. The modification of gCN has been sought as an alternative approach to utilize this material to develop tissue-engineered platforms. There are no reports of gCN incorporated 3D printed platforms for biomedical applications. However, researchers have explored the 3D printing of gCN composites with polymers such as sodium alginate to develop the aerogel membranes for wastewater remediation during direct ink writing. This strategy could potentially be transitioned to biomedical applications to develop a well-designed platform based on gCN.

8. MXenes

MXenes are a relatively newer class of ultrathin 2D nanomaterials (transition metal carbides, nitrides, or carbonitrides) discovered in 2011 [165,166]. MXene has a structural formula of $M_{n+1}X_nT_x$ where ‘M’ refers to the transition metal, ‘X’ refers to carbon or nitrogen, and ‘T’ refers to the terminal groups such as –O, –OH, or –F [167]. With the emergence of theranostic nanomedicine platforms based on 2D nanomaterials, MXenes have been explored for biosensing, bioimaging, and photothermal therapy platforms [168–170]. The room temperature sensing ability of MXenes, compared to higher temperature metal oxide semiconductors-based sensing, and their suitable bandgap than that of graphene, has led to a newly found attraction of researchers in the biosensing field using MXenes [171]. The biocompatibility and high photothermal efficiency of MXenes at NIR bio-window have recently attracted researchers’ attention in TERM [165,172]. Furthermore, the degradation of MXene after interaction with water and oxygen yields non-hazardous byproducts such as CO_2 or N_2. Additionally, for MXenes with bioactive transition elements such as titanium, the degradation product promotes bone tissue regeneration [173].

3D printable MXene inks have been developed in pure suspension form or combination with binders for inkjet printing and screen printing, mostly for industrial applications [174,175]. $Ti_3C_2T_x$ based aqueous suspension (minimum 50 mg/ml concentration) had suitable rheological properties for extrusion printing. Though such structures were shown to be suitable for electronic applications [176,177], the attractive biological properties of MXenes have also inspired their utilization for the development of 3D printed scaffolds with multi-functionalities for biomedical applications. Pan et al. integrated Ti_3C_2 MXene with bioactive glass (BG) ceramics for extrusion printing of porous BG scaffolds with both tumor ablation and bone regeneration capabilities (Fig. 12A). The results showed the NIR-induced photothermal effect, and eventual ablation of tumors in mice after MXene incorporated scaffolds were implanted. Though BG-based scaffolds have osteogenic properties by themselves, this hybridization was observed to promote their osteogenic capabilities further as indicated by a higher bone formation in MXene incorporated groups [172].

Another biomedical application for MXene based platform encompasses the development of wearable medical devices [178,179]. Like graphene, MXene has favorable electronic properties and can transduce the pressure signals, making it suitable for developing high sensitive pressure sensors [179]. Its attractive bending strength empowers the development of flexible substrates to develop flexible 3D printed wearable devices (Fig. 12B–C). These devices can be implanted on the skin, joints, or muscles to capture mechanistic signals facilitated by the piezoresistive phenomenon of MXenes. The printable ink based on aqueous suspension or in combination with other materials such as oxidized cellulose has been developed for stimuli-responsive platforms.

9. Outlook on the toxicity of 2D nanomaterials

2D nanomaterials have become more widely studied for their potential biomedical applications and 3D printing technologies. Graphene quantum dots (GQDs), not discussed earlier, have shown low toxicity *in vitro* and *in vivo* [180–182]. GQDs have been shown to accumulate in treated mice's liver, spleen, lung, and kidney, but no significant toxicity or organ damage has been reported [182].

Studies comparing graphene and its derivative graphene oxide have reported size-dependent toxicity with small and large sizes of both materials reducing cell viability via increased DNA damage and ROS generation in zebrafish [183]. In mice, there have been opposing findings of the toxicity of graphene and its derivatives. Park et al. showed a subchronic inflammatory response in mice with commercially available graphene nanoplates (GNPs) [181], while Singh et al. found a thrombo-protective effect following intravenous (IV) administration of amine-modified graphene in mice [180] as compared to GO and rGO. Thus, these previous studies suggest potentially safer modifications of graphene for *in vivo* biomedical applications.

Moreover, GO has demonstrated dose-dependent cytotoxicity as supported by i*n vitro* studies in HeLa cells [184] as well as potential antibacterial activity [185,186], although other studies suggest no noticeable antimicrobial effect with GO alone against *E. co*li and *P. aeruginosa* [187]. Similar antibacterial activity with low cytotoxicity has been reported using rGO in *E. coli* [188]. *In vivo*, higher doses of GO have been shown to induce chronic toxicity in the lung, liver, spleen, and kidney, as well as inflammatory responses in mice [184,189]. An et al. showed that short-term repeated GO exposure could result in multiple ocular inflammatory findings, but these findings were not present with rGO in mice [190]. Similarly, Hasan et al. did not find a preliminary toxic response to rGO-derived GQDs in mice [191]. Whether graphene and its derivatives have a cytotoxic effect in humans is still to be further elucidated.

Laponite clay studies have revealed selective cytotoxicity towards cancer cells while proving relatively safe in concentrations less than 1 mg/ml in human MSC [192] and as implantable bioceramics in rats [193]. As shown from the studies outlined in Table 1, Laponite's low cytotoxicity proposes clay materials as safe alternatives for drug delivery and other biomedical applications. Other clays, such as MMT, have been researched extensively to prevent aflatoxin toxicity in mice and rats at low concentrations [194,195]. MMT has also

been shown to decrease biomarkers of aflatoxin exposure in studies of Ghanaians at high risk of aflatoxicosis [196]. Certain modifications of MMT have proven to be less toxic than other modifications, as outlined in Supplementary Table 1. Overall, 2D silicate clays appear to have either no or low toxicity at concentrations studied and have already shown promising applications related to preventing aflatoxin toxicity in humans.

TMDs and TMOs have shown various toxic effects depending on which transition metal is used [197] and whether it has been modified [198]. For instance, WS_2 appears to elicit slightly more toxic responses than MoS_2 and WS_2, which some studies have found to be safe and less hazardous [199]. Moreover, PEGylated MoS_2, WS_2, and TiS_2 nanosheets appear to have no appreciable *in vitro* toxicity even at higher concentrations (200 μg/ml) [200].

Antibacterial activity has been shown in multiple studies of hBN [201–203]. Mild cytotoxic and dose-dependent cytotoxicity has been found with hBN materials and potential inflammatory response and damage to main organs such as the liver, kidney, heart, spleen, and pancreas in studies with mice and rats, respectively [204,205].

Lastly, 2D nanomaterials, including BP, gCN, and MXenes, have shown promising biomedical applications like wound healing and tissue regeneration with no or low toxic effects, particularly *in vitro* [206–208]. While some studies have shown nephrotoxicity with BP and toxicity with multiple administrations of BP [209,210], other studies have not found long-term pathological damage to main organs [211]. Similarly, *in vitro* studies of graphitic carbon nitride appear to show no or low cytotoxicity, but more research is needed to confirm these findings *in vivo*. MXenes are a fast-growing family of 2D nanomaterials that have expanded the number of compositions that can be synthesized. Toxicity studies of MXenes have shown no or low cytotoxicity, as shown in Table 1. Many of these explored compositions of MXenes have a unique combination of properties that could be used for biomedical applications and offer newer alternatives to existing treatments [166]. In conclusion, the studies highlighted in Table 1 and Supplementary Table 1 largely indicate potentially safe applications of these 2D nanomaterials. However, more studies in larger animals and a better understanding of toxicities are needed before newer biomedical applications of these 2D nanomaterials are developed for the patients.

10. Outlook and conclusion

There have been significant individual research interests in both 2D nanomaterials and 3D printing for biomedical applications. The convergence of these two research topics has resulted in several novel approaches to tissue-engineered scaffolds and therapeutic platforms. Design flexibility and rationality enabled by 3D printing technologies have resulted in the development of constructs with proper orientation and assembly of 2D nanomaterials to leverage their unraveled properties for a range of healthcare applications. One emerging trend in this area is the development of multifunctional platforms with both therapeutic and regenerative potential. Certain 2D nanomaterials, due to their unique photoabsorption properties and inherent bioactivities, have been combined with 3D printable polymers to develop these platforms. 3D printed constructs with BP, TMDs, and MXenes

have all found interest in photothermal and photodynamic therapy of bone tumors and eventual promotion of bone regeneration at tumor resection site. With the perpetual advancements in 3D printing technologies and classes of 2D nanomaterials, the converged research on these areas is expected to soar for the years.

Among the several classes of 2D nanomaterials, silicate clays have attracted significant attention for extrusion-based 3D bioprinting applications. The aqueous rheological properties of these materials, combined with their cytocompatibility, have been leveraged to develop the bioprinted cell-laden constructs for TERM. Furthermore, the mineral composition of clays has been demonstrated to induce osteogenic activities desired for bone tissue engineering, and its surface chemistry makes it an ideal material to bind growth factors and drugs for the development of sustained-release platforms. As such, silicate clays hold great potential to improve the 3D printability of existing biocompatible hydrogels for tissue engineering, wound healing, and drug delivery applications. Furthermore, the excellent retention of growth factors and drugs, owing to the unique surface property of clays, can be utilized to develop robust *in vitro* drug testing cell-laden platforms.

Here, we attempted to review the most recent advances in 3D printing and bioprinting with emerging 2D nanomaterials and highlighted the multifunctionalities imparted by these materials to such printed constructs for biomedical applications. Graphene and its family, and silicate clays have been the focal point of research in 3D printing and bioprinting. However, several other 2D nanomaterials have emerged over the years and been combined with existing 3D printable materials to add the dynamism in biomaterial design and applications. With the exceptional properties of 2D nanomaterials along with the unprecedented potential of additive manufacturing in designing and molding materials to clinically relevant structures, an enormous opportunity lies ahead for the development of next-generation regenerative approaches, cancer therapies, drug delivery platforms, biosensors, and bioelectronics.

Supplementary Material

Refer to Web version on PubMed Central for supplementary material.

Acknowledgements

This work was supported by the National Institute of Health Grant R01 AR75037.

Data availability statement

No data is available for this publication.

List of abbreviation

2D	Two-dimensional
3D	Three-dimensional
GO	Graphene Oxide

rGO	Reduced Graphene Oxide
BP	Black Phosphorus
TMD	Transition Metal Dichalcogenide
TMO	Transition Metal Oxide
hBN	Hexagonal Boron Nitride
TERM	Tissue Engineering and Regenerative Medicine
MSC	Mesenchymal Stem Cells
NIR	Near-Infrared
UV	Ultraviolet
RANKL/OPG	Receptor Activator of Nuclear factor Kappa-B Ligand/ Osteoprotegerin
Ti, V, Mo, W	Titanium, Vanadium, Molybdenum, Tungsten
S, Se, Te	Sulfur, Selenium, Tellurium
PCL	Polycaprolactone
PLGA	Poly(lactic-co-glycolic acid)
GelMa	Gelatin Methacrylate
PEG	Polyethylene glycol
PVP	Polyvinylpyrrolidone

References

[1]. Geim AK, Novoselov KS, The rise of graphene, Nat. Mater 6 (3) (2007) 183–191. [PubMed: 17330084]

[2]. Xu M, Liang T, Shi M, Chen H, Graphene-like two-dimensional materials, Chem. Rev 113 (5) (2013) 3766–3798. [PubMed: 23286380]

[3]. Balandin AA, Thermal properties of graphene and nanostructured carbon materials, Nat. Mater 10 (8) (2011) 569–581. [PubMed: 21778997]

[4]. Castro Neto AH, Guinea F, Peres NMR, Novoselov KS, Geim AK, The electronic properties of graphene, Rev. Mod. Phys 81 (1) (2009) 109–162.

[5]. Novoselov KS, Geim AK, Morozov SV, Jiang D, Zhang Y, Dubonos SV, Grigorieva IV, Firsov AA, Electric field effect in atomically thin carbon films, Science 306 (5696) (2004) 666–669. [PubMed: 15499015]

[6]. The rise of two-dimensional materials, Accounts Chem. Res 48 (1) (2015) 1–2.

[7]. Velický M, Toth PS, From two-dimensional materials to their heterostructures: an electrochemist's perspective, Appl. Mater. Today 8 (2017) 68–103.

[8]. Khan K, Tareen AK, Aslam M, Wang R, Zhang Y, Mahmood A, Ouyang Z, Zhang H, Guo Z, Recent developments in emerging two-dimensional materials and their applications, J. Mater. Chem C 8 (2) (2020) 387–440.

[9]. Cheng J, Wang C, Zou X, Liao L, Recent advances in optoelectronic devices based on 2D materials and their heterostructures, Adv. Opt. Mater 7 (1) (2019) 1800441.

[10]. Lemme MC, Wagner S, Lee K, Fan X, Verbiest GJ, Wittmann S, Lukas S, Dolleman RJ, Niklaus F, van der Zant HSJ, Duesberg GS, Steeneken PG, Nanoelectromechanical sensors based on suspended 2D materials, Research 2020 (2020) 8748602. [PubMed: 32766550]

[11]. Deng D, Novoselov KS, Fu Q, Zheng N, Tian Z, Bao X, Catalysis with two-dimensional materials and their heterostructures, Nat. Nanotechnol 11 (3) (2016) 218–230. [PubMed: 26936816]

[12]. Liu Y, Peng X, Recent advances of supercapacitors based on two-dimensional materials, Appl. Mater. Today 8 (2017) 104–115.

[13]. Ye C, Chao D, Shan J, Li H, Davey K, Qiao S-Z, Unveiling the advances of 2D materials for Li/Na-S batteries experimentally and theoretically, Matter 2 (2) (2020) 323–344.

[14]. Rohaizad N, Mayorga-Martinez CC, Fojtů M, Latiff NM, Pumera M, Two-dimensional materials in biomedical, biosensing and sensing applications, Chem. Soc. Rev 50 (1) (2021) 619–657. [PubMed: 33206730]

[15]. Zhang H, Fan T, Chen W, Li Y, Wang B, Recent advances of two-dimensional materials in smart drug delivery nano-systems, Bioact. Mater 5 (4) (2020) 1071–1086. [PubMed: 32695937]

[16]. Bolotsky A, Butler D, Dong C, Gerace K, Glavin NR, Muratore C, Robinson JA, Ebrahimi A, Two-dimensional materials in biosensing and healthcare: from in vitro diagnostics to optogenetics and beyond, ACS Nano 13 (9) (2019) 9781–9810. [PubMed: 31430131]

[17]. Cheng L, Wang X, Gong F, Liu T, Liu Z, 2D nanomaterials for cancer theranostic applications, Adv. Mater 32 (13) (2020) 1902333.

[18]. Zheng Y, Hong X, Wang J, Feng L, Fan T, Guo R, Zhang H, 2D nanomaterials for tissue engineering and regenerative nanomedicines: recent advances and future challenges, Adv. Healthcare Mater 10 (7) (2021) 2001743.

[19]. Lalwani G, Henslee AM, Farshid B, Lin L, Kasper FK, Qin Y-X, Mikos AG, Sitharaman B, Two-dimensional nanostructure-reinforced biodegradable polymeric nanocomposites for bone tissue engineering, Biomacromolecules 14 (3) (2013) 900–909. [PubMed: 23405887]

[20]. Ventola CL, Medical applications for 3D printing: current and projected uses, P T 39 (10) (2014) 704–711. [PubMed: 25336867]

[21]. Chia HN, Wu BM, Recent advances in 3D printing of biomaterials, J. Biol. Eng 9 (1) (2015) 4. [PubMed: 25866560]

[22]. Prendergast ME, Burdick JA, Recent advances in enabling technologies in 3D printing for precision medicine, Adv. Mater 32 (13) (2020) 1902516.

[23]. Murphy SV, Atala A, 3D bioprinting of tissues and organs, Nat. Biotechnol 32 (8) (2014) 773–785. [PubMed: 25093879]

[24]. Freeman FE, Pitacco P, van Dommelen LHA, Nulty J, Browe DC, Shin J-Y, Alsberg E, Kelly DJ, 3D bioprinting spatiotemporally defined patterns of growth factors to tightly control tissue regeneration, Sci. Adv 6 (33) (2020) eabb5093. [PubMed: 32851179]

[25]. Kim JH, Seol Y-J, Ko IK, Kang H-W, Lee YK, Yoo JJ, Atala A, Lee SJ, 3D bioprinted human skeletal muscle constructs for muscle function restoration, Sci. Rep 8 (1) (2018) 12307. [PubMed: 30120282]

[26]. Kim JH, Kim I, Seol Y-J, Ko IK, Yoo JJ, Atala A, Lee SJ, Neural cell integration into 3D bioprinted skeletal muscle constructs accelerates restoration of muscle function, Nat. Commun 11 (1) (2020) 1025. [PubMed: 32094341]

[27]. Ma X, Liu J, Zhu W, Tang M, Lawrence N, Yu C, Gou M, Chen S, 3D bioprinting of functional tissue models for personalized drug screening and in vitro disease modeling, Adv. Drug Deliv. Rev 132 (2018) 235–251. [PubMed: 29935988]

[28]. Jorgensen AM, Yoo JJ, Atala A, Solid organ bioprinting: strategies to achieve organ function, Chem. Rev 120 (19) (2020) 11093–11127. [PubMed: 32885956]

[29]. Leberfinger AN, Dinda S, Wu Y, Koduru SV, Ozbolat V, Ravnic DJ, Ozbolat IT, Bioprinting functional tissues, Acta Biomater. 95 (2019) 32–49. [PubMed: 30639351]

[30]. Sha J, Li Y, Villegas Salvatierra R, Wang T, Dong P, Ji Y, Lee S-K, Zhang C, Zhang J, Smith RH, Ajayan PM, Lou J, Zhao N, Tour JM, Three-dimensional printed graphene foams, ACS Nano 11 (7) (2017) 6860–6867. [PubMed: 28608675]

[31]. Jakus AE, Secor EB, Rutz AL, Jordan SW, Hersam MC, Shah RN, Three-dimensional printing of high-content graphene scaffolds for electronic and biomedical applications, ACS Nano 9 (4) (2015) 4636–4648. [PubMed: 25858670]

[32]. Jiang Y, Xu Z, Huang T, Liu Y, Guo F, Xi J, Gao W, Gao C, Direct 3D printing of ultralight graphene oxide aerogel microlattices, Adv. Funct. Mater 28 (16) (2018) 1707024.

[33]. Zhu C, Han TY-J, Duoss EB, Golobic AM, Kuntz JD, Spadaccini CM, Worsley MA, Highly compressible 3D periodic graphene aerogel microlattices, Nat. Commun 6 (1) (2015) 6962. [PubMed: 25902277]

[34]. Daukiya L, Seibel J, De Feyter S, Chemical modification of 2D materials using molecules and assemblies of molecules, Adv. Phys X 4 (1) (2019) 1625723.

[35]. Placone JK, Engler AJ, Recent advances in extrusion-based 3D printing for biomedical applications, Adv. Healthcare Mater 7 (8) (2018) 1701161.

[36]. Wu G-H, S.-h. Hsu, Review: polymeric-based 3D printing for tissue engineering, J. Med. Biol. Eng 35 (3) (2015) 285–292. [PubMed: 26167139]

[37]. Chimene D, Alge DL, Gaharwar AK, Two-dimensional nanomaterials for biomedical applications: emerging trends and future prospects, Adv. Mater 27 (45) (2015) 7261–7284. [PubMed: 26459239]

[38]. Three-dimensional bioprinting of anatomically realistic tissue constructs for disease modeling and drug testing, Tissue Eng. C Methods 27 (3) (2021) 225–231.

[39]. Peng W, Unutmaz D, Ozbolat IT, Bioprinting towards physiologically relevant tissue models for pharmaceutics, Trends Biotechnol. 34 (9) (2016) 722–732. [PubMed: 27296078]

[40]. Zhang Y, Yu Y, Chen H, Ozbolat IT, Characterization of printable cellular micro-fluidic channels for tissue engineering, Biofabrication 5 (2) (2013) 25004.

[41]. Chimene D, Lennox KK, Kaunas RR, Gaharwar AK, Advanced bioinks for 3D printing: a materials science perspective, Ann. Biomed. Eng 44 (6) (2016) 2090–2102. [PubMed: 27184494]

[42]. Chimene D, Kaunas R, Gaharwar AK, Hydrogel bioink reinforcement for additive manufacturing: a focused review of emerging strategies, Adv. Mater 32 (1) (2020) 1902026.

[43]. Gaharwar AK, Cross LM, Peak CW, Gold K, Carrow JK, Brokesh A, Singh KA, 2D nanoclay for biomedical applications: regenerative medicine, therapeutic delivery, and additive manufacturing, Adv. Mater 31 (23) (2019) 1900332.

[44]. Zhang J, Eyisoylu H, Qin X-H, Rubert M, Müller R, 3D bioprinting of graphene oxide-incorporated cell-laden bone mimicking scaffolds for promoting scaffold fidelity, osteogenic differentiation and mineralization, Acta Biomater. 121 (2020) 637–652, 10.1016/j.actbio.2020.12.026. [PubMed: 33326888]

[45]. Kinloch IA, Suhr J, Lou J, Young RJ, Ajayan PM, Composites with carbon nanotubes and graphene: an outlook, Science 362 (6414) (2018) 547–553. [PubMed: 30385571]

[46]. Cheng C, Li S, Thomas A, Kotov NA, Haag R, Functional graphene nanomaterials based architectures: biointeractions, fabrications, and emerging biological applications, Chem. Rev 117 (3) (2017) 1826–1914. [PubMed: 28075573]

[47]. Jakus AE, Shah RN, Multi and mixed 3D-printing of graphene-hydroxyapatite hybrid materials for complex tissue engineering, J. Biomed. Mater. Res 105 (1) (2017) 274–283.

[48]. Novel poly(ϵ-caprolactone)/graphene scaffolds for bone cancer treatment and bone regeneration, 3D Print. Addit. Manuf 7 (5) (2020) 222–229. [PubMed: 33134427]

[49]. 3D-Printed poly(ϵ-caprolactone)/graphene scaffolds activated with P1-latex protein for bone regeneration, 3D Print. Addit. Manuf 5 (2) (2018) 127–137.

[50]. Wang W, Junior JRP, Nalesso PRL, Musson D, Cornish J, Mendonça F, Caetano GF, Bártolo P, Engineered 3D printed poly(ϵ-caprolactone)/graphene scaffolds for bone tissue engineering, Mater. Sci. Eng. C 100 (2019) 759–770.

[51]. Zhu Y, Murali S, Cai W, Li X, Suk JW, Potts JR, Ruoff RS, Graphene and graphene oxide: synthesis, properties, and applications, Adv. Mater 22 (35) (2010) 3906–3924. [PubMed: 20706983]

[52]. Georgakilas V, Otyepka M, Bourlinos AB, Chandra V, Kim N, Kemp KC, Hobza P, Zboril R, Kim KS, Functionalization of graphene: covalent and non-covalent approaches, derivatives and applications, Chem. Rev 112 (11) (2012) 6156–6214. [PubMed: 23009634]

[53]. Chen D, Feng H, Li J, Graphene oxide: preparation, functionalization, and electrochemical applications, Chem. Rev 112 (11) (2012) 6027–6053. [PubMed: 22889102]

[54]. Worsley MA, Kucheyev SO, Mason HE, Merrill MD, Mayer BP, Lewicki J, Valdez CA, Suss ME, Stadermann M, Pauzauskie PJ, Satcher JH, Biener J, Baumann TF, Mechanically robust 3D graphene macroassembly with high surface area, Chem. Commun 48 (67) (2012) 8428–8430.

[55]. Worsley MA, Pauzauskie PJ, Olson TY, Biener J, Satcher JH, Baumann TF, Synthesis of graphene aerogel with high electrical conductivity, J. Am. Chem. Soc 132 (40) (2010) 14067–14069. [PubMed: 20860374]

[56]. Qing H, Ji Y, Li W, Zhao G, Yang Q, Zhang X, Luo Z, Lu TJ, Jin G, Xu F, Microfluidic printing of three-dimensional graphene electroactive microfibrous scaffolds, ACS Appl. Mater. Interfaces 12 (2) (2020) 2049–2058. [PubMed: 31799832]

[57]. Wang F, Jiang Y, Liu Y, Guo F, Fang W, Xu Z, Gao C, Liquid crystalline 3D printing for superstrong graphene microlattices with high density, Carbon 159 (2020) 166–174.

[58]. García-Tuñón E, Feilden E, Zheng H, D'Elia E, Leong A, Saiz E, Graphene oxide: an all-in-one processing additive for 3D printing, ACS Appl. Mater. Interfaces 9 (38) (2017) 32977–32989. [PubMed: 28898053]

[59]. Lu R, Zhang W, He Y, et al. , Ferric ion crosslinking-based 3D printing of a graphene oxide hydrogel and its evaluation as a bio-scaffold in tissue engineering, Biotechnol. Bioeng 118 (2021) 1006–1012, 10.1002/bit.27592. [PubMed: 33022744]

[60]. Li M, Xiong P, Yan F, Li S, Ren C, Yin Z, Li A, Li H, Ji X, Zheng Y, Cheng Y, An overview of graphene-based hydroxyapatite composites for orthopedic applications, Bioact. Mater 3 (1) (2018) 1–18. [PubMed: 29744438]

[61]. Yi J, Choe G, Park J, Lee JY, Graphene oxide-incorporated hydrogels for biomedical applications, Polym. J 52 (8) (2020) 823–837.

[62]. Zhang Y, Zhai D, Xu M, Yao Q, Zhu H, Chang J, Wu C, 3D-printed bioceramic scaffolds with antibacterial and osteogenic activity, Biofabrication 9 (2) (2017) 25037.

[63]. Olate-Moya F, Arens L, Wilhelm M, Mateos-Timoneda MA, Engel E, Palza H, Chondroinductive alginate-based hydrogels having graphene oxide for 3D printed scaffold fabrication, ACS Appl. Mater. Interfaces 12 (4) (2020) 4343–4357. [PubMed: 31909967]

[64]. Zhou X, Nowicki M, Cui H, Zhu W, Fang X, Miao S, Lee S-J, Keidar M, Zhang LG, 3D bioprinted graphene oxide-incorporated matrix for promoting chondrogenic differentiation of human bone marrow mesenchymal stem cells, Carbon 116 (2017) 615–624.

[65]. Belaid H, Nagarajan S, Teyssier C, Barou C, Baŕes J, Balme S, Garay H, Huon V, Cornu D, Cavaillès V, Bechelany M, Development of new biocompatible 3D printed graphene oxide-based scaffolds, Mater. Sci. Eng. C 110 (2020) 110595.

[66]. Boga JC, Miguel SP, de Melo-Diogo D, Mendonça AG, Louro RO, Correia IJ, In vitro characterization of 3D printed scaffolds aimed at bone tissue regeneration, Colloids Surf. B Biointerfaces 165 (2018) 207–218. [PubMed: 29486449]

[67]. Shuai C, Feng P, Gao C, Shuai X, Xiao T, Peng S, Graphene oxide reinforced poly(vinyl alcohol): nanocomposite scaffolds for tissue engineering applications, RSC Adv. 5 (32) (2015) 25416–25423.

[68]. Wu C, Xia L, Han P, Xu M, Fang B, Wang J, Chang J, Xiao Y, Graphene-oxide-modified β-tricalcium phosphate bioceramics stimulate in vitro and in vivo osteogenesis, Carbon 93 (2015) 116–129.

[69]. Unagolla JM, Jayasuriya AC, Enhanced cell functions on graphene oxide incorporated 3D printed polycaprolactone scaffolds, Mater. Sci. Eng. C 102 (2019) 1–11.

[70]. Cheng Z, Xigong L, Weiyi D, Jingen H, Shuo W, Xiangjin L, Junsong W, Potential use of 3D-printed graphene oxide scaffold for construction of the cartilage layer, J. Nanobiotechnol 18 (1) (2020) 97.

[71]. Melo SF, Neves SC, Pereira AT, Borges I, Granja PL, Magalhães FD, Gonçalves IC, Incorporation of graphene oxide into poly(ϵ-caprolactone) 3D printed fibrous scaffolds improves their antimicrobial properties, Mater. Sci. Eng. C 109 (2020) 110537.

[72]. Liu X, Miller AL, Park S, George MN, Waletzki BE, Xu H, Terzic A, Lu L, Two-dimensional black phosphorus and graphene oxide nanosheets synergistically enhance cell proliferation and osteogenesis on 3D printed scaffolds, ACS Appl. Mater. Interfaces 11 (26) (2019) 23558–23572. [PubMed: 31199116]

[73]. Zhang Z, Jørgensen ML, Wang Z, Amagat J, Wang Y, Li Q, Dong M, Chen M, 3D anisotropic photocatalytic architectures as bioactive nerve guidance conduits for peripheral neural regeneration, Biomaterials 253 (2020) 120108. [PubMed: 32428776]

[74]. Qian Y, Zhao X, Han Q, Chen W, Li H, Yuan W, An integrated multi-layer 3D-fabrication of PDA/RGD coated graphene loaded PCL nanoscaffold for peripheral nerve restoration, Nat. Commun 9 (1) (2018) 323. [PubMed: 29358641]

[75]. Choe G, Oh S, Seok JM, Park SA, Lee JY, Graphene oxide/alginate composites as novel bioinks for three-dimensional mesenchymal stem cell printing and bone regeneration applications, Nanoscale 11 (48) (2019) 23275–23285. [PubMed: 31782460]

[76]. Wang Y, Chen Y, Lacey SD, Xu L, Xie H, Li T, Danner VA, Hu L, Reduced graphene oxide film with record-high conductivity and mobility, Mater. Today 21 (2) (2018) 186–192.

[77]. Smith AT, LaChance AM, Zeng S, Liu B, Sun L, Synthesis, properties, and applications of graphene oxide/reduced graphene oxide and their nanocomposites, Nano Mater. Sci 1 (1) (2019) 31–47.

[78]. Zhou M, Zhai Y, Dong S, Electrochemical sensing and biosensing platform based on chemically reduced graphene oxide, Anal. Chem 81 (14) (2009) 5603–5613. [PubMed: 19522529]

[79]. Yan M, Liu Y, Zhu X, Wang X, Liu L, Sun H, Wang C, Kong D, Ma G, Nanoscale reduced graphene oxide-mediated photothermal therapy together with IDO inhibition and PD-L1 blockade synergistically promote antitumor immunity, ACS Appl. Mater. Interfaces 11 (2) (2019) 1876–1885. [PubMed: 30582788]

[80]. Shin SR, Li Y-C, Jang HL, Khoshakhlagh P, Akbari M, Nasajpour A, Zhang YS, Tamayol A, Khademhosseini A, Graphene-based materials for tissue engineering, Adv. Drug Deliv. Rev 105 (2016) 255–274. [PubMed: 27037064]

[81]. Fang J-H, Hsu H-H, Hsu R-S, Peng C-K, Lu Y-J, Chen Y-Y, Chen S-Y, Hu S-H, 4D printing of stretchable nanocookie@conduit material hosting biocues and magnetoelectric stimulation for neurite sprouting, NPG Asia Mater. 12 (1) (2020) 61.

[82]. Wang J, Wang H, Mo X, Wang H, Reduced graphene oxide-encapsulated microfiber patterns enable controllable formation of neuronal-like networks, Adv. Mater 32 (40) (2020) 2004555.

[83]. Lima-Sousa R, de Melo-Diogo D, Alves CG, Cabral CSD, Miguel SP, Mendonça AG, Correia IJ, Injectable in situ forming thermo-responsive graphene based hydrogels for cancer chemo-photothermal therapy and NIR light-enhanced antibacterial applications, Mater. Sci. Eng. C 117 (2020) 111294.

[84]. Vijayavenkataraman S, Thaharah S, Zhang S, Lu WF, Fuh JYH, 3D-Printed PCL/rGO conductive scaffolds for peripheral nerve injury repair, Artif. Organs 43 (5) (2019) 515–523.

[85]. Kim JH, Chang WS, Kim D, Yang JR, Han JT, Lee G-W, Kim JT, Seol SK, 3D printing of reduced graphene oxide nanowires, Adv. Mater 27 (1) (2015) 157–161. [PubMed: 25393844]

[86]. Golzar H, Mohammadrezaei D, Yadegari A, Rasoulianboroujeni M, Hashemi M, Omidi M, Yazdian F, Shalbaf M, Tayebi L, Incorporation of functionalized reduced graphene oxide/magnesium nanohybrid to enhance the osteoinductivity capability of 3D printed calcium phosphate-based scaffolds, Compos. B Eng 185 (2020) 107749.

[87]. Cabral CSD, Miguel SP, de Melo-Diogo D, Louro RO, Correia IJ, Green reduced graphene oxide functionalized 3D printed scaffolds for bone tissue regeneration, Carbon 146 (2019) 513–523.

[88]. Page DJ, Clarkin CE, Mani R, Khan NA, Dawson JI, Evans ND, Injectable nanoclay gels for angiogenesis, Acta Biomater. 100 (2019) 378–387. [PubMed: 31541735]

[89]. Cross LM, Carrow JK, Ding X, Singh KA, Gaharwar AK, Sustained and prolonged delivery of protein therapeutics from two-dimensional nanosilicates, ACS Appl. Mater. Interfaces 11 (7) (2019) 6741–6750. [PubMed: 30676016]

[90]. Wilson SA, Cross LM, Peak CW, Gaharwar AK, Shear-thinning and thermo-reversible nanoengineered inks for 3D bioprinting, ACS Appl. Mater. Interfaces 9 (50) (2017) 43449–43458. [PubMed: 29214803]

[91]. Gao Q, Niu X, Shao L, Zhou L, Lin Z, Sun A, Fu J, Chen Z, Hu J, Liu Y, He Y, 3D printing of complex GelMA-based scaffolds with nanoclay, Biofabrication 11 (3) (2019), 035006. [PubMed: 30836349]

[92]. Habib MA, Khoda B, Development of clay based novel bio-ink for 3D bioprinting process, Procedia Manuf. 26 (2018) 846–856.

[93]. Wei J, Wang B, Li Z, Wu Z, Zhang M, Sheng N, Liang Q, Wang H, Chen S, A 3D-printable TEMPO-oxidized bacterial cellulose/alginate hydrogel with enhanced stability via nanoclay incorporation, Carbohydr. Polym 238 (2020) 116207. [PubMed: 32299554]

[94]. Cai F-F, Heid S, Boccaccini AR, Potential of Laponite® incorporated oxidized alginate–gelatin (ADA-GEL) composite hydrogels for extrusion-based 3D printing, J. Biomed. Mater. Res 109 (2021) 1090–1104, 10.1002/jbm.b.34771.

[95]. Dávila JL, d'Ávila MA, Rheological evaluation of Laponite/alginate inks for 3D extrusion-based printing, Int. J. Adv. Manuf. Technol 101 (1) (2019) 675–686.

[96]. Jin Y, Liu C, Chai W, Compaan A, Huang Y, Self-supporting nanoclay as internal scaffold material for direct printing of soft hydrogel composite structures in air, ACS Appl. Mater. Interfaces 9 (20) (2017) 17456–17465. [PubMed: 28467835]

[97]. Afghah F, Altunbek M, Dikyol C, Koc B, Preparation and characterization of nanoclay-hydrogel composite support-bath for bioprinting of complex structures, Sci. Rep 10 (1) (2020) 5257. [PubMed: 32210259]

[98]. Adib AA, Sheikhi A, Shahhosseini M, Simeunovíc A, Wu S, Castro CE, Zhao R, Khademhosseini A, Hoelzle DJ, Direct-write 3D printing and characterization of a GelMA-based biomaterial for intracorporeal tissue engineering, Biofabrication 12 (4) (2020) 45006.

[99]. Chimene D, Peak CW, Gentry JL, Carrow JK, Cross LM, Mondragon E, Cardoso GB, Kaunas R, Gaharwar AK, Nanoengineered ionic–covalent entanglement (NICE) bioinks for 3D bioprinting, ACS Appl. Mater. Interfaces 10 (12) (2018) 9957–9968. [PubMed: 29461795]

[100]. Sears C, Mondragon E, Richards ZI, Sears N, Chimene D, McNeill EP, Gregory CA, Gaharwar AK, Kaunas R, Conditioning of 3D printed nanoengineered ionic–covalent entanglement scaffolds with iP-hMSCs derived matrix, Adv. Healthcare Mater 9 (15) (2020) 1901580.

[101]. Chimene D, Miller L, Cross LM, Jaiswal MK, Singh I, Gaharwar AK, Nanoengineered osteoinductive bioink for 3D bioprinting bone tissue, ACS Appl. Mater. Interfaces 12 (14) (2020) 15976–15988. [PubMed: 32091189]

[102]. Peak CW, Singh KA, Adlouni M.a., Chen J, Gaharwar AK, Printing therapeutic proteins in 3D using nanoengineered bioink to control and direct cell migration, Adv. Healthcare Mater 8 (11) (2019) 1801553.

[103]. Liang Q, Gao F, Zeng Z, Yang J, Wu M, Gao C, Cheng D, Pan H, Liu W, Ruan C, Coaxial scale-up printing of diameter-tunable biohybrid hydrogel microtubes with high strength, perfusability, and endothelialization, Adv. Funct. Mater 30 (43) (2020) 2001485.

[104]. Cidonio G, Cooke M, Glinka M, Dawson JI, Grover L, Oreffo ROC, Printing bone in a gel: using nanocomposite bioink to print functionalised bone scaffolds, Mater. Today Bio 4 (2019) 100028.

[105]. Carrow JK, Di Luca A, Dolatshahi-Pirouz A, Moroni L, Gaharwar AK, 3D-printed bioactive scaffolds from nanosilicates and PEOT/PBT for bone tissue engineering, Regen. Biomater 6 (1) (2018) 29–37. [PubMed: 30740240]

[106]. Ahlfeld T, Cidonio G, Kilian D, Duin S, Akkineni AR, Dawson JI, Yang S, Lode A, Oreffo ROC, Gelinsky M, Development of a clay based bioink for 3D cell printing for skeletal application, Biofabrication 9 (3) (2017), 034103. [PubMed: 28691691]

[107]. Cebe T, Ahuja N, Monte F, Awad K, Vyavhare K, Aswath P, Huang J, Brotto M, Varanasi V, Novel 3D-printed methacrylated chitosan-laponite nanosilicate composite scaffolds enhance cell growth and biomineral formation in MC3T3 pre-osteoblasts, J. Mater. Res 35 (2018) 1–18.

[108]. Zhai X, Ruan C, Ma Y, Cheng D, Wu M, Liu W, Zhao X, Pan H, Lu WW, 3D Bioprinted osteoblast-laden nanocomposite hydrogel constructs with induced microenvironments promote

cell viability, differentiation, and osteogenesis both in vitro and in vivo, Adv. Sci 5 (3) (2018) 1700550.

[109]. Peak CW, Stein J, Gold KA, Gaharwar AK, Nanoengineered colloidal inks for 3D bioprinting, Langmuir 34 (3) (2018) 917–925. [PubMed: 28981287]

[110]. Tabriz AG, Hermida MA, Leslie NR, Shu W, Three-dimensional bioprinting of complex cell laden alginate hydrogel structures, Biofabrication 7 (4) (2015) 45012.

[111]. Weng Z, Wang J, Senthil T, Wu L, Mechanical and thermal properties of ABS/montmorillonite nanocomposites for fused deposition modeling 3D printing, Mater. Des 102 (2016) 276–283.

[112]. Eng H, Maleksaeedi S, Yu S, Choong YYC, Wiria FE, Tan CLC, Su PC, Wei J, 3D stereolithography of polymer composites reinforced with orientated nanoclay, Procedia Eng. 216 (2017) 1–7.

[113]. Coppola B, Cappetti N, Di Maio L, Scarfato P, Incarnato L, 3D printing of PLA/clay nanocomposites: influence of printing temperature on printed samples properties, Materials 11 (10) (2018) 1947. [PubMed: 30314390]

[114]. Gaihre B, Liu X, Tilton M, Li L, Li Y, Lu L, Spatial and uniform deposition of cell-laden constructs on 3D printed composite phosphorylated hydrogels for improved osteoblast responses, J. Mater. Sci 56 (31) (2021) 17768–17784.

[115]. Habib A, Khoda B, Development of clay based novel hybrid bio-ink for 3D bioprinting process, J. Manuf. Process 38 (2019) 76–87.

[116]. Cui Z-K, Kim S, Baljon JJ, Wu BM, Aghaloo T, Lee M, Microporous methacrylated glycol chitosan-montmorillonite nanocomposite hydrogel for bone tissue engineering, Nat. Commun 10 (1) (2019) 3523. [PubMed: 31388014]

[117]. Wang H, Yang X, Shao W, Chen S, Xie J, Zhang X, Wang J, Xie Y, Ultrathin black phosphorus nanosheets for efficient singlet oxygen generation, J. Am. Chem. Soc 137 (35) (2015) 11376–11382. [PubMed: 26284535]

[118]. Xu Y, Wang Z, Guo Z, Huang H, Xiao Q, Zhang H, Yu X-F, Solvothermal synthesis and ultrafast photonics of black phosphorus quantum dots, Adv. Opt. Mater 4 (8) (2016) 1223–1229.

[119]. Watts MC, Picco L, Russell-Pavier FS, Cullen PL, Miller TS, Bartús SP, Payton OD, Skipper NT, Tileli V, Howard CA, Production of phosphorene nanoribbons, Nature 568 (7751) (2019) 216–220. [PubMed: 30971839]

[120]. Hou J, Wang H, Ge Z, Zuo T, Chen Q, Liu X, Mou S, Fan C, Xie Y, Wang L, Treating acute kidney injury with antioxidative black phosphorus nanosheets, Nano Lett. 20 (2) (2020) 1447–1454. [PubMed: 31975594]

[121]. Huang K, Wu J, Gu Z, Black phosphorus hydrogel scaffolds enhance bone regeneration via a sustained supply of calcium-free phosphorus, ACS Appl. Mater. Interfaces 11 (3) (2019) 2908–2916. [PubMed: 30596421]

[122]. Raucci MG, Fasolino I, Caporali M, Serrano-Ruiz M, Soriente A, Peruzzini M, Ambrosio L, Exfoliated black phosphorus promotes in vitro bone regeneration and suppresses osteosarcoma progression through cancer-related inflammation inhibition, ACS Appl. Mater. Interfaces 11 (9) (2019) 9333–9342. [PubMed: 30758933]

[123]. Wang Y, Hu X, Zhang L, Zhu C, Wang J, Li Y, Wang Y, Wang C, Zhang Y, Yuan Q, Bioinspired extracellular vesicles embedded with black phosphorus for molecular recognition-guided biomineralization, Nat. Commun 10 (1) (2019) 2829. [PubMed: 31249296]

[124]. Wang Z, Zhao J, Tang W, Hu L, Chen X, Su Y, Zou C, Wang J, Lu WW, Zhen W, Zhang R, Yang D, Peng S, Multifunctional nanoengineered hydrogels consisting of black phosphorus nanosheets upregulate bone formation, Small 15 (41) (2019) 1901560.

[125]. Chen W, Ouyang J, Yi X, Xu Y, Niu C, Zhang W, Wang L, Sheng J, Deng L, Liu YN, Guo S, Black phosphorus nanosheets as a neuroprotective nanomedicine for neurodegenerative disorder therapy, Adv. Mater 30 (3) (2018) 1703458.

[126]. Qian Y, Yuan W-E, Cheng Y, Yang Y, Qu X, Fan C, Concentrically integrative bioassembly of a three-dimensional black phosphorus nanoscaffold for restoring neurogenesis, angiogenesis, and immune homeostasis, Nano Lett. 19 (12) (2019) 8990–9001. [PubMed: 31790262]

[127]. Huang X-W, Wei J-J, Zhang M-Y, Zhang X-L, Yin X-F, Lu C-H, Song J-B, Bai S-M, Yang H-H, Water-based black phosphorus hybrid nanosheets as a moldable platform for wound healing applications, ACS Appl. Mater. Interfaces 10 (41) (2018) 35495–35502. [PubMed: 30251823]

[128]. Luo M, Fan T, Zhou Y, Zhang H, Mei L, 2D black phosphorus–based biomedical applications, Adv. Funct. Mater 29 (13) (2019) 1808306.

[129]. Yang B, Yin J, Chen Y, Pan S, Yao H, Gao Y, Shi J, 2D-Black-Phosphorus-Reinforced 3D-printed scaffolds:A stepwise countermeasure for osteosarcoma, Adv. Mater 30 (10) (2018) 1705611.

[130]. Wang C, Ye X, Zhao Y, Bai L, He Z, Tong Q, Xie X, Zhu H, Cai D, Zhou Y, Lu B, Wei Y, Mei L, Xie D, Wang M, Cryogenic 3D printing of porous scaffolds for in situ delivery of 2D black phosphorus nanosheets, doxorubicin hydrochloride and osteogenic peptide for treating tumor resection-induced bone defects, Biofabrication 12 (3) (2020), 035004. [PubMed: 31952065]

[131]. Cheng L, Cai Z, Zhao J, Wang F, Lu M, Deng L, Cui W, Black phosphorus-based 2D materials for bone therapy, Bioact. Mater 5 (4) (2020) 1026–1043. [PubMed: 32695934]

[132]. Zhang YJ, Ideue T, Onga M, Qin F, Suzuki R, Zak A, Tenne R, Smet JH, Iwasa Y, Enhanced intrinsic photovoltaic effect in tungsten disulfide nanotubes, Nature 570 (7761) (2019) 349–353.

[133]. Choi W, Choudhary N, Han GH, Park J, Akinwande D, Lee YH, Recent development of two-dimensional transition metal dichalcogenides and their applications, Mater. Today 20 (3) (2017) 116–130.

[134]. Wang S, Li K, Chen Y, Chen H, Ma M, Feng J, Zhao Q, Shi J, Biocompatible PEGylated MoS2 nanosheets: controllable bottom-up synthesis and highly efficient photothermal regression of tumor, Biomaterials 39 (2015) 206–217. [PubMed: 25468372]

[135]. Han J, Xia H, Wu Y, Kong SN, Deivasigamani A, Xu R, Hui KM, Kang Y, Single-layer MoS2 nanosheet grafted upconversion nanoparticles for near-infrared fluorescence imaging-guided deep tissue cancer phototherapy, Nanoscale 8 (15) (2016) 7861–7865. [PubMed: 27035265]

[136]. Palumbo A, Tourlomousis F, Chang RC, Yang E-H, Influence of transition metal dichalcogenide surfaces on cellular morphology and adhesion, ACS Appl. Bio Mater 1 (5) (2018) 1448–1457.

[137]. Wang H, Zeng X, Pang L, Wang H, Lin B, Deng Z, Qi ELX, Miao N, Wang D, Huang P, Hu H, Li J, Integrative treatment of anti-tumor/bone repair by combination of MoS2 nanosheets with 3D printed bioactive borosilicate glass scaffolds, Chem. Eng. J 396 (2020) 125081.

[138]. Wang X, Li T, Ma H, Zhai D, Jiang C, Chang J, Wang J, Wu C, A 3D-printed scaffold with MoS2 nanosheets for tumor therapy and tissue regeneration, NPG Asia Mater. 9 (4) (2017) e376–e376.

[139]. Chen Y-W, Shie M-Y, Hsiao C-H, Liang Y-C, Wang B, Chen IWP, Synthesis of high-quality monolayer tungsten disulfide with chlorophylls and its application for enhancing bone regeneration, npj 2D Mater. Appl 4 (1) (2020) 34.

[140]. Lalwani G, Henslee AM, Farshid B, Parmar P, Lin L, Qin Y-X, Kasper FK, Mikos AG, Sitharaman B, Tungsten disulfide nanotubes reinforced biodegradable polymers for bone tissue engineering, Acta Biomater. 9 (9) (2013) 8365–8373. [PubMed: 23727293]

[141]. Kalantar-zadeh K, Ou JZ, Daeneke T, Mitchell A, Sasaki T, Fuhrer MS, Two dimensional and layered transition metal oxides, Appl. Mater. Today 5 (2016) 73–89.

[142]. Yang J, Zeng Z, Kang J, Betzler S, Czarnik C, Zhang X, Ophus C, Yu C, Bustillo K, Pan M, Qiu J, Wang L-W, Zheng H, Formation of two-dimensional transition metal oxide nanosheets with nanoparticles as intermediates, Nat. Mater 18 (9) (2019) 970–976. [PubMed: 31285617]

[143]. Walia S, Balendhran S, Nili H, Zhuiykov S, Rosengarten G, Wang QH, Bhaskaran M, Sriram S, Strano MS, Kalantar-zadeh K, Transition metal oxides – thermoelectric properties, Prog. Mater. Sci 58 (8) (2013) 1443–1489.

[144]. Ren B, Wang Y, Ou JZ, Engineering two-dimensional metal oxides via surface functionalization for biological applications, J. Mater. Chem. B 8 (6) (2020) 1108–1127. [PubMed: 31971200]

[145]. Yuan D, Ding L, Sun Z, Li X, MRI/Fluorescence bimodal amplification system for cellular GSH detection and tumor cell imaging based on manganese dioxide nanosheet, Sci. Rep 8 (1) (2018) 1747. [PubMed: 29379132]

[146]. Zhang M, Xing L, Ke H, He Y-J, Cui P-F, Zhu Y, Jiang G, Qiao J-B, Lu N, Chen H, Jiang H-L, MnO2-Based nanoplatform serves as drug vehicle and MRI contrast agent for cancer theranostics, ACS Appl. Mater. Interfaces 9 (13) (2017) 11337–11344. [PubMed: 28291320]

[147]. Fu C, Duan X, Cao M, Jiang S, Ban X, Guo N, Zhang F, Mao J, Huyan T, Shen J, Zhang LM, Targeted magnetic resonance imaging and modulation of hypoxia with multifunctional hyaluronic acid-MnO2 nanoparticles in glioma, Adv. Healthcare Mater 8 (10) (2019) 1900047.

[148]. Chen Y, Ye D, Wu M, Chen H, Zhang L, Shi J, Wang L, Break-up of two-dimensional MnO2 nanosheets promotes ultrasensitive pH-triggered theranostics of cancer, Adv. Mater 26 (41) (2014) 7019–7026. [PubMed: 25156250]

[149]. Yao B, Chandrasekaran S, Zhang J, Xiao W, Qian F, Zhu C, Duoss EB, Spadaccini CM, Worsley MA, Li Y, Efficient 3D printed pseudocapacitive electrodes with ultrahigh MnO2 loading, Joule 3 (2) (2019) 459–470.

[150]. Wang X, Zheng S, Zhou F, Qin J, Shi X, Wang S, Sun C, Bao X, Wu Z-S, Scalable fabrication of printed Zn//MnO2 planar micro-batteries with high volumetric energy density and exceptional safety, Natl. Sci. Rev 7 (1) (2019) 64–72. [PubMed: 34692018]

[151]. Jafari S, Mahyad B, Hashemzadeh H, Janfaza S, Gholikhani T, Tayebi L, Biomedical applications of TiO(2) nanostructures: recent advances, Int. J. Nanomed 15 (2020) 3447–3470.

[152]. Hou Z, Zhang Y, Deng K, Chen Y, Li X, Deng X, Cheng Z, Lian H, Li C, Lin J, UV-emitting upconversion-based TiO2 photosensitizing nanoplatform: near-infrared light mediated in vivo photodynamic therapy via mitochondria-involved apoptosis pathway, ACS Nano 9 (3) (2015) 2584–2599. [PubMed: 25692960]

[153]. Moosavi MA, Sharifi M, Ghafary SM, Mohammadalipour Z, Khataee A, Rahmati M, Hajjaran S, Łos MJ, Klonisch T, Ghavami S, Photodynamic N TiO2 nanoparticle treatment induces controlled ROS-mediated autophagy and terminal differentiation of leukemia cells, Sci. Rep 6 (1) (2016) 34413. [PubMed: 27698385]

[154]. You DG, Deepagan VG, Um W, Jeon S, Son S, Chang H, Yoon HI, Cho YW, Swierczewska M, Lee S, Pomper MG, Kwon IC, Kim K, Park JH, ROS-generating TiO2 nanoparticles for non-invasive sonodynamic therapy of cancer, Sci. Rep 6 (1) (2016) 23200. [PubMed: 26996446]

[155]. Dean D, Wallace J, Siblani A, Wang MO, Kim K, Mikos AG, Fisher JP, Continuous digital light processing (cDLP): highly accurate additive manufacturing of tissue engineered bone scaffolds, Virtual Phys. Prototyp 7 (1) (2012) 13–24. [PubMed: 23066427]

[156]. Mott EJ, Busso M, Luo X, Dolder C, Wang MO, Fisher JP, Dean D, Digital micromirror device (DMD)-based 3D printing of poly(propylene fumarate) scaffolds, Mater. Sci. Eng. C 61 (2016) 301–311.

[157]. Rasoulianboroujeni M, Fahimipour F, Shah P, Khoshroo K, Tahriri M, Eslami H, Yadegari A, Dashtimoghadam E, Tayebi L, Development of 3D-printed PLGA/TiO2 nanocomposite scaffolds for bone tissue engineering applications, Mater. Sci. Eng. C 96 (2019) 105–113.

[158]. Jackson RJ, Patrick PS, Page K, Powell MJ, Lythgoe MF, Miodownik MA, Parkin IP, Carmalt CJ, Kalber TL, Bear JC, Chemically treated 3D printed polymer scaffolds for biomineral formation, ACS Omega 3 (4) (2018) 4342–4351. [PubMed: 29732454]

[159]. Zhu X, Ng LWT, Hu G, Wu T-C, Um D-S, Macadam N, Hasan T, Hexagonal boron nitride–enhanced optically transparent polymer dielectric inks for printable electronics, Adv. Funct. Mater 30 (31) (2020) 2002339. [PubMed: 32774201]

[160]. Woosley S, Galehdari NA, Kelkar A, Aravamudhan S, Fused deposition modeling 3D printing of boron nitride composites for neutron radiation shielding, J. Mater. Res 33 (22) (2018) 3657–3664.

[161]. Merlo A, Mokkapati VRSS, Pandit S, Mijakovic I, Boron nitride nanomaterials: biocompatibility and bio-applications, Biomater. Sci 6 (9) (2018) 2298–2311. [PubMed: 30059084]

[162]. Guiney LM, Mansukhani ND, Jakus AE, Wallace SG, Shah RN, Hersam MC, Three-dimensional printing of cytocompatible, thermally conductive hexagonal boron nitride nanocomposites, Nano Lett. 18 (6) (2018) 3488–3493. [PubMed: 29709193]

[163]. Aki D, Ulag S, Unal S, Sengor M, Ekren N, Lin C-C, Yılmazer H, Ustundag CB, Kalaskar DM, Gunduz O, 3D printing of PVA/hexagonal boron nitride/bacterial cellulose composite scaffolds for bone tissue engineering, Mater. Des 196 (2020) 109094.

[164]. Belaid H, Nagarajan S, Barou C, Huon V, Bares J, Balme S, Miele P, Cornu D, Cavaillès V, Teyssier C, Bechelany M, Boron nitride based nanobiocomposites: design by 3D printing for bone tissue engineering, ACS Appl. Bio Mater 3 (4) (2020) 1865–1874.

[165]. Sreenilayam SP, Ul Ahad I, Nicolosi V, Brabazon D, MXene materials based printed flexible devices for healthcare, biomedical and energy storage applications, Mater. Today 43 (2021) 99–131.

[166]. Gogotsi Y, Anasori B, The rise of MXenes, ACS Nano 13 (8) (2019) 8491–8494. [PubMed: 31454866]

[167]. Anasori B, Lukatskaya MR, Gogotsi Y, 2D metal carbides and nitrides (MXenes) for energy storage, Nat. Rev. Mater 2 (2) (2017) 16098.

[168]. Ji X, Ge L, Liu C, Tang Z, Xiao Y, Chen W, Lei Z, Gao W, Blake S, De D, Shi B, Zeng X, Kong N, Zhang X, Tao W, Capturing functional two-dimensional nanosheets from sandwich-structure vermiculite for cancer theranostics, Nat. Commun 12 (1) (2021) 1124. [PubMed: 33602928]

[169]. Huang K, Li Z, Lin J, Han G, Huang P, Two-dimensional transition metal carbides and nitrides (MXenes) for biomedical applications, Chem. Soc. Rev 47 (14) (2018) 5109–5124. [PubMed: 29667670]

[170]. Soleymaniha M, Shahbazi M-A, Rafieerad AR, Maleki A, Amiri A, Promoting role of MXene nanosheets in biomedical sciences: therapeutic and biosensing innovations, Adv. Healthcare Mater 8 (1) (2019) 1801137.

[171]. Xu B, Zhu M, Zhang W, Zhen X, Pei Z, Xue Q, Zhi C, Shi P, Ultrathin MXenemicropattern-based field-effect transistor for probing neural activity, Adv. Mater 28 (17) (2016) 3333–3339. [PubMed: 26924616]

[172]. Pan S, Yin J, Yu L, Zhang C, Zhu Y, Gao Y, Chen Y, 2D MXene-integrated 3D-printing scaffolds for augmented osteosarcoma phototherapy and accelerated tissue reconstruction, Adv. Sci 7 (2) (2020) 1901511.

[173]. Zhang CJ, Pinilla S, McEvoy N, Cullen CP, Anasori B, Long E, Park S-H, Seral-Ascaso A, Shmeliov A, Krishnan D, Morant C, Liu X, Duesberg GS, Gogotsi Y, Nicolosi V, Oxidation stability of colloidal two-dimensional titanium carbides (MXenes), Chem. Mater 29 (11) (2017) 4848–4856.

[174]. Wu C-W, Unnikrishnan B, Chen IWP, Harroun SG, Chang H-T, Huang C-C, Excellent oxidation resistive MXene aqueous ink for micro-supercapacitor application, Energy Storage Mater. 25 (2020) 563–571.

[175]. Li H, Li X, Liang J, Chen Y, Hydrous RuO2-decorated MXene coordinating with silver nanowire inks enabling fully printed micro-supercapacitors with extraordinary volumetric performance, Adv. Energy Mater 9 (15) (2019) 1803987.

[176]. Yang W, Yang J, Byun JJ, Moissinac FP, Xu J, Haigh SJ, Domingos M, Bissett MA, Dryfe RAW, Barg S, 3D printing of freestanding MXene architectures for current-collector-free supercapacitors, Adv. Mater 31 (37) (2019) 1902725.

[177]. Orangi J, Hamade F, Davis VA, Beidaghi M, 3D printing of additive-free 2D Ti3C2Tx (MXene) ink for fabrication of micro-supercapacitors with ultra-high energy densities, ACS Nano 14 (1) (2020) 640–650. [PubMed: 31891247]

[178]. Cheng Y, Ma Y, Li L, Zhu M, Yue Y, Liu W, Wang L, Jia S, Li C, Qi T, Wang J, Gao Y, Bioinspired microspines for a high-performance spray Ti3C2Tx MXene-based piezoresistive sensor, ACS Nano 14 (2) (2020) 2145–2155. [PubMed: 32040310]

[179]. Guo Y, Zhong M, Fang Z, Wan P, Yu G, A wearable transient pressure sensor made with MXene nanosheets for sensitive broad-range human–machine interfacing, Nano Lett. 19 (2) (2019) 1143–1150. [PubMed: 30657695]

[180]. Singh SK, Singh MK, Kulkarni PP, Sonkar VK, Gŕacio JJA, Dash D, Aminemodified graphene: thrombo-protective safer alternative to graphene oxide for biomedical applications, ACS Nano 6 (3) (2012) 2731–2740. [PubMed: 22376049]

[181]. Park E-J, Lee G-H, Han BS, Lee B-S, Lee S, Cho M-H, Kim J-H, Kim D-W, Toxic response of graphene nanoplatelets in vivo and in vitro, Arch. Toxicol 89 (9) (2015) 1557–1568. [PubMed: 24980260]

[182]. Nurunnabi M, Khatun Z, Huh KM, Park SY, Lee DY, Cho KJ, Lee Y.-k., In vivo biodistribution and toxicology of carboxylated graphene quantum dots, ACS Nano 7 (8) (2013) 6858–6867. [PubMed: 23829293]

[183]. Jia P-P, Sun T, Junaid M, Yang L, Ma Y-B, Cui Z-S, Wei D-P, Shi H-F, Pei D-S, Nanotoxicity of different sizes of graphene (G) and graphene oxide (GO) in vitro and in vivo, Environ. Pollut 247 (2019) 595–606. [PubMed: 30708322]

[184]. Yang K, Li Y, Tan X, Peng R, Liu Z, Behavior and toxicity of graphene and its functionalized derivatives in biological systems, Small 9 (9–10) (2013) 1492–1503. [PubMed: 22987582]

[185]. Hu W, Peng C, Luo W, Lv M, Li X, Li D, Huang Q, Fan C, Graphene-based antibacterial paper, ACS Nano 4 (7) (2010) 4317–4323. [PubMed: 20593851]

[186]. Chook SW, Chia CH, Sarani Z, Ayob MK, Chee KL, Neoh HM, Huang NM, Silver nanoparticles - graphene oxide nanocomposite for antibacterial purpose, Adv. Mater. Res 364 (2012) 439–443.

[187]. Das MR, Sarma RK, Saikia R, Kale VS, Shelke MV, Sengupta P, Synthesis of silver nanoparticles in an aqueous suspension of graphene oxide sheets and its antimicrobial activity, Colloids Surf. B Biointerfaces 83 (1) (2011) 16–22. [PubMed: 21109409]

[188]. Liu S, Zeng TH, Hofmann M, Burcombe E, Wei J, Jiang R, Kong J, Chen Y, Antibacterial activity of graphite, graphite oxide, graphene oxide, and reduced graphene oxide: membrane and oxidative stress, ACS Nano 5 (9) (2011) 6971–6980. [PubMed: 21851105]

[189]. Wang K, Ruan J, Song H, Zhang J, Wo Y, Guo S, Cui D, Biocompatibility of graphene oxide, Nanoscale Res. Lett 6 (1) (2010) 8. [PubMed: 27502632]

[190]. An W, Zhang Y, Zhang X, Li K, Kang Y, Akhtar S, Sha X, Gao L, Ocular toxicity of reduced graphene oxide or graphene oxide exposure in mouse eyes, Exp. Eye Res 174 (2018) 59–69. [PubMed: 29803558]

[191]. Hasan MT, Lee BH, Lin C-W, McDonald-Boyer A, Gonzalez-Rodriguez R, Vasireddy S, Tsedev U, Coffer J, Belcher AM, Naumov AV, Near-infrared emitting graphene quantum dots synthesized from reduced graphene oxide for in vitro/in vivo/ex vivo bioimaging applications, 2D Mater. 8 (3) (2021) 35013.

[192]. Gaharwar AK, Mihaila SM, Swami A, Patel A, Sant S, Reis RL, Marques AP, Gomes ME, Khademhosseini A, Bioactive silicate nanoplatelets for osteogenic differentiation of human mesenchymal stem cells, Adv. Mater 25 (24) (2013) 3329–3336. [PubMed: 23670944]

[193]. Wang C, Wang S, Li K, Ju Y, Li J, Zhang Y, Li J, Liu X, Shi X, Zhao Q, Preparation of laponite bioceramics for potential bone tissue engineering applications, PLoS One 9 (6) (2014) e99585. [PubMed: 24955961]

[194]. Nye E, Feist-Burkhardt S, Horne DJ, Ross AJ, Whittaker JE, The palaeoenvironment associated with a partial iguanodon skeleton from the upper weald clay (barremian, early cretaceous) at smokejacks brickworks (ockley, surrey, UK), based on palynomorphs and ostracods, Cretac. Res 29 (3) (2008) 417–444.

[195]. Baek M, Lee J-A, Choi S-J, Toxicological effects of a cationic clay, montmorillonite in vitro and in vivo, Mol. Cell. Toxicol 8 (1) (2012) 95–101.

[196]. Phillips TD, Wang M, Elmore SE, Hearon S, Wang J-S, NovaSil clay for the protection of humans and animals from aflatoxins and other contaminants, Clay Clay Miner. 67 (1) (2019) 99–110.

[197]. Ivask A, Titma T, Visnapuu M, Vija H, Kakinen A, Sihtmae M, Pokhrel S, Madler L, Heinlaan M, Kisand V, Shimmo R, Kahru A, Toxicity of 11 metal oxide nanoparticles to three mammalian cell types *in Vitro*, Curr. Top. Med. Chem 15 (18) (2015) 1914–1929. [PubMed: 25961521]

[198]. Singh AK, Yadav AN, Srivastav S, Jaiswal RK, Srivastava A, Mondal AC, Singh K, CdSe-Reduced graphene oxide nanocomposite toxicity alleviation via V2O5 shell formation over CdSe core: in vivo and in vitro studies, Nanotechnology 31 (41) (2020) 415101. [PubMed: 32311687]

[199]. Anju S, Mohanan PV, Biomedical applications of transition metal dichalcogenides (TMDCs), Synth. Met 271 (2021) 116610.

[200]. Hao J, Song G, Liu T, Yi X, Yang K, Cheng L, Liu Z, In vivo long-term biodistribution, excretion, and toxicology of PEGylated transition-metal dichalcogenides MS2 (M = Mo, W, Ti) nanosheets, Adv. Sci 4 (1) (2017) 1600160.

[201]. Zhang Y, Chan C, Li Z, Ma J, Meng Q, Zhi C, Sun H, Fan J, Nanotoxicity of boron nitride nanosheet to bacterial membranes, Langmuir 35 (18) (2019) 6179–6187. [PubMed: 30955333]

[202]. Pandit S, Gaska K, Mokkapati VRSS, Forsberg S, Svensson M, Kádár R, Mijakovic I, Antibacterial effect of boron nitride flakes with controlled orientation in polymer composites, RSC Adv. 9 (57) (2019) 33454–33459. [PubMed: 35529107]

[203]. Mukheem A, Shahabuddin S, Akbar N, Miskon A, Muhamad Sarih N, Sudesh K, Ahmed Khan N, Saidur R, Sridewi N, Boron nitride doped polyhydroxyalkanoate/chitosan nanocomposite for antibacterial and biological applications, Nanomaterials 9 (4) (2019) 645. [PubMed: 31010071]

[204]. Kodali VK, Roberts JR, Shoeb M, Wolfarth MG, Bishop L, Eye T, Barger M, Roach KA, Friend S, Schwegler-Berry D, Chen BT, Stefaniak A, Jordan KC, Whitney RR, Porter DW, Erdely AD, Acute in vitro and in vivo toxicity of a commercial grade boron nitride nanotube mixture, Nanotoxicology 11 (8) (2017) 1040–1058. [PubMed: 29094619]

[205]. Santos J, Moschetta M, Rodrigues J, Alpuim P, Capasso A, Interactions between 2D materials and living matter: a review on graphene and hexagonal boron nitride coatings, Front. Bioeng. Biotechnol 9 (5) (2021).

[206]. Xie H, Shao J, Ma Y, Wang J, Huang H, Yang N, Wang H, Ruan C, Luo Y, Wang QQ, Chu PK, Yu X-F, Biodegradable near-infrared-photoresponsive shape memory implants based on black phosphorus nanofillers, Biomaterials 164 (2018) 11–21. [PubMed: 29477708]

[207]. Zhang J, Fu Y, Mo A, Multilayered titanium carbide MXene film for guided bone regeneration, Int. J. Nanomed 14 (2019) 10091–10103.

[208]. Shao J, Xie H, Huang H, Li Z, Sun Z, Xu Y, Xiao Q, Yu X-F, Zhao Y, Zhang H, Wang H, Chu PK, Biodegradable black phosphorus-based nanospheres for in vivo photothermal cancer therapy, Nat. Commun 7 (1) (2016) 12967. [PubMed: 27686999]

[209]. He C, Ruan F, Jiang S, Zeng J, Yin H, Liu R, Zhang Y, Huang L, Wang C, Ma S, Zuo Z, Black phosphorus quantum dots cause nephrotoxicity in organoids, mice, and human cells, Small 16 (22) (2020) 2001371.

[210]. Sun Y, Fan S, Fan S, Li C, Shang Z, Gu M, Liang S, Tian X, In vitro and in vivo toxicity of black phosphorus nanosheets, J. Nanosci. Nanotechnol 20 (2) (2020) 659–667. [PubMed: 31383060]

[211]. Mu X, Wang J-Y, Bai X, Xu F, Liu H, Yang J, Jing Y, Liu L, Xue X, Dai H, Liu Q, Sun Y-M, Liu C, Zhang X-D, Black phosphorus quantum dot induced oxidative stress and toxicity in living cells and mice, ACS Appl. Mater. Interfaces 9 (24) (2017) 20399–20409. [PubMed: 28553710]

[212]. Chong Y, Ma Y, Shen H, Tu X, Zhou X, Xu J, Dai J, Fan S, Zhang Z, The in vitro and in vivo toxicity of graphene quantum dots, Biomaterials 35 (19) (2014) 5041–5048. [PubMed: 24685264]

[213]. Zhang S, Yang K, Feng L, Liu Z, In vitro and in vivo behaviors of dextran functionalized graphene, Carbon 49 (12) (2011) 4040–4049.

[214]. Chang Y, Yang S-T, Liu J-H, Dong E, Wang Y, Cao A, Liu Y, Wang H, In vitro toxicity evaluation of graphene oxide on A549 cells, Toxicol. Lett 200 (3) (2011) 201–210. [PubMed: 21130147]

[215]. Jaworski S, Sawosz E, Kutwin M, Wierzbicki M, Hinzmann M, Grodzik M, Winnicka A, Lipińska L, Włodyga K, Chwalibog A, In vitro and in vivo effects of graphene oxide and reduced graphene oxide on glioblastoma, Int. J. Nanomed 10 (2015) 1585–1596.

[216]. Tomás H, Alves CS, Rodrigues J, Laponite®, A key nanoplatform for biomedical applications? Nanomed. Nanotechnol. Biol. Med 14 (7) (2018) 2407–2420.

[217]. Maisanaba S, Pichardo S, Puerto M, Gutíerrez-Praena D, Cameán AM, Jos A, Toxicological evaluation of clay minerals and derived nanocomposites: a review, Environ. Res 138 (2015) 233–254. [PubMed: 25732897]

[218]. Shi YH, Xu ZR, Feng JL, Wang CZ, Efficacy of modified montmorillonite nanocomposite to reduce the toxicity of aflatoxin in broiler chicks, Anim. Feed Sci. Technol 129 (1) (2006) 138–148.

[219]. Sun Y, Fan S, Fan S, Li C, Shang Z, Gu M, Liang S, Tian X, In vitro and in vivo toxicity of black phosphorus nanosheets, J. Nanosci. Nanotechnol 20 (2) (2020) 659–667. [PubMed: 31383060]

[220]. Sobańska Z, Zapór L, Szparaga M, Stępnik M, Biological effects of molybdenum compounds in nanosized forms under in vitro and in vivo conditions, Int. J. Occup. Med. Environ. Health 33 (1) (2020) 1–19. [PubMed: 31749447]

[221]. Gu M, Dai Z, Yan X, Ma J, Niu Y, Lan W, Wang X, Xu Q, Comparison of toxicity of Ti3C2 and Nb2C Mxene quantum dots (QDs) to human umbilical vein endothelial cells, J. Appl. Toxicol 41 (5) (2021) 745–754. [PubMed: 33048420]

[222]. Lim GP, Soon CF, Ma NL, Morsin M, Nayan N, Ahmad MK, Tee KS, Cytotoxicity of MXene-based nanomaterials for biomedical applications: a mini review, Environ. Res 201 (2021) 111592. [PubMed: 34175291]

[223]. Hussein EA, Zagho MM, Rizeq BR, Younes NN, Pintus G, Mahmoud KA, Nasrallah GK, Elzatahry AA, Plasmonic MXene-based nanocomposites exhibiting photothermal therapeutic effects with lower acute toxicity than pure MXene, Int. J. Nanomed 14 (2019) 4529–4539.

[224]. Alhussain H, Augustine R, Hussein EA, Gupta I, Hasan A, Al Moustafa AE, Elzatahry A, MXene nanosheets may induce toxic effect on the early stage of embryogenesis, J. Biomed. Nanotechnol 16 (3) (2020) 364–372. [PubMed: 32493546]

[225]. Nasrallah GK, Al-Asmakh M, Rasool K, Mahmoud KA, Ecotoxicological assessment of Ti3C2Tx (MXene) using a zebrafish embryo model, Environ. Sci. Nano 5 (4) (2018) 1002–1011.

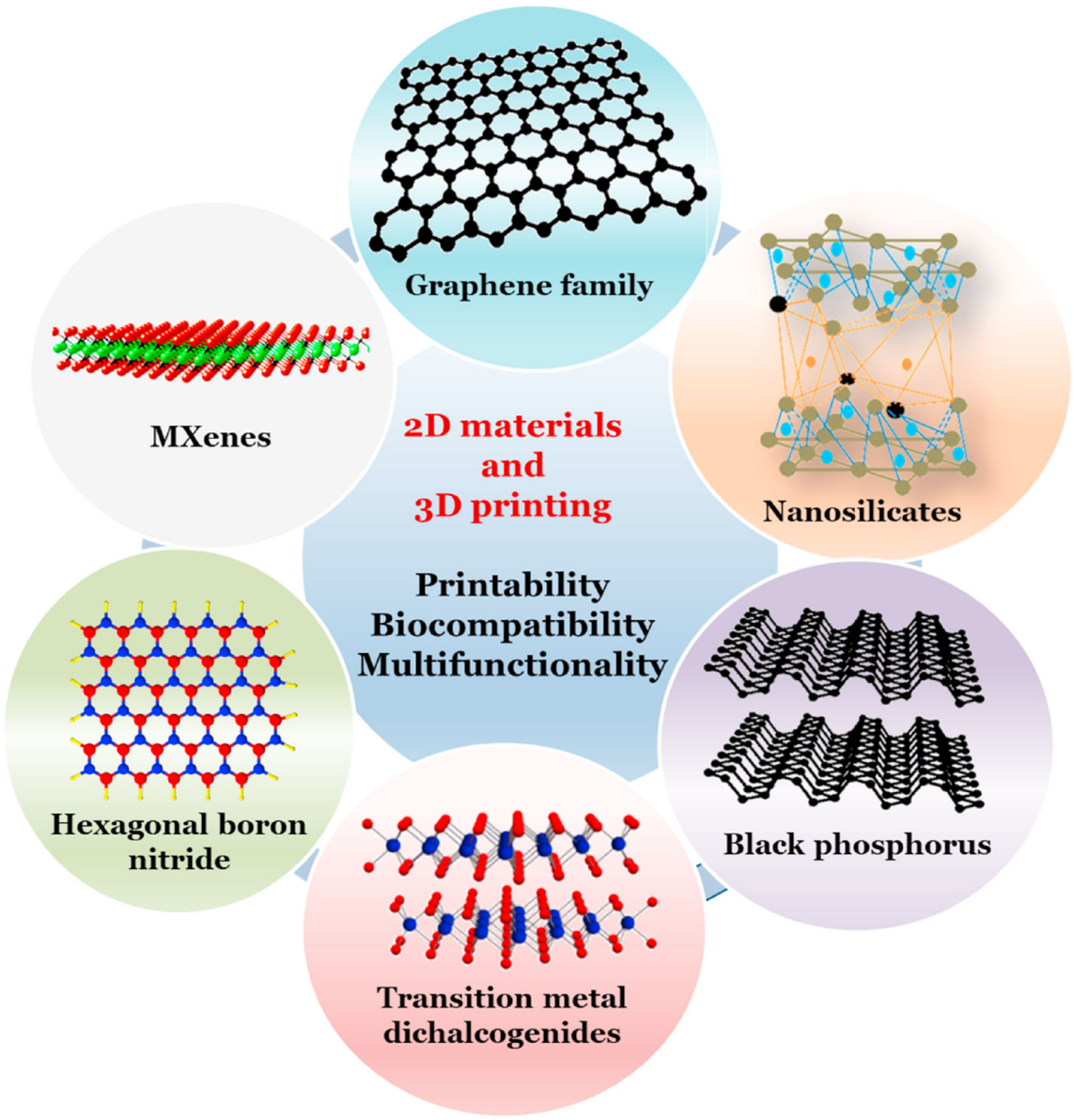

Fig. 1.

Schematics showing common 2D nanomaterials currently used in 3D printing of multifunctional and biocompatible platforms.

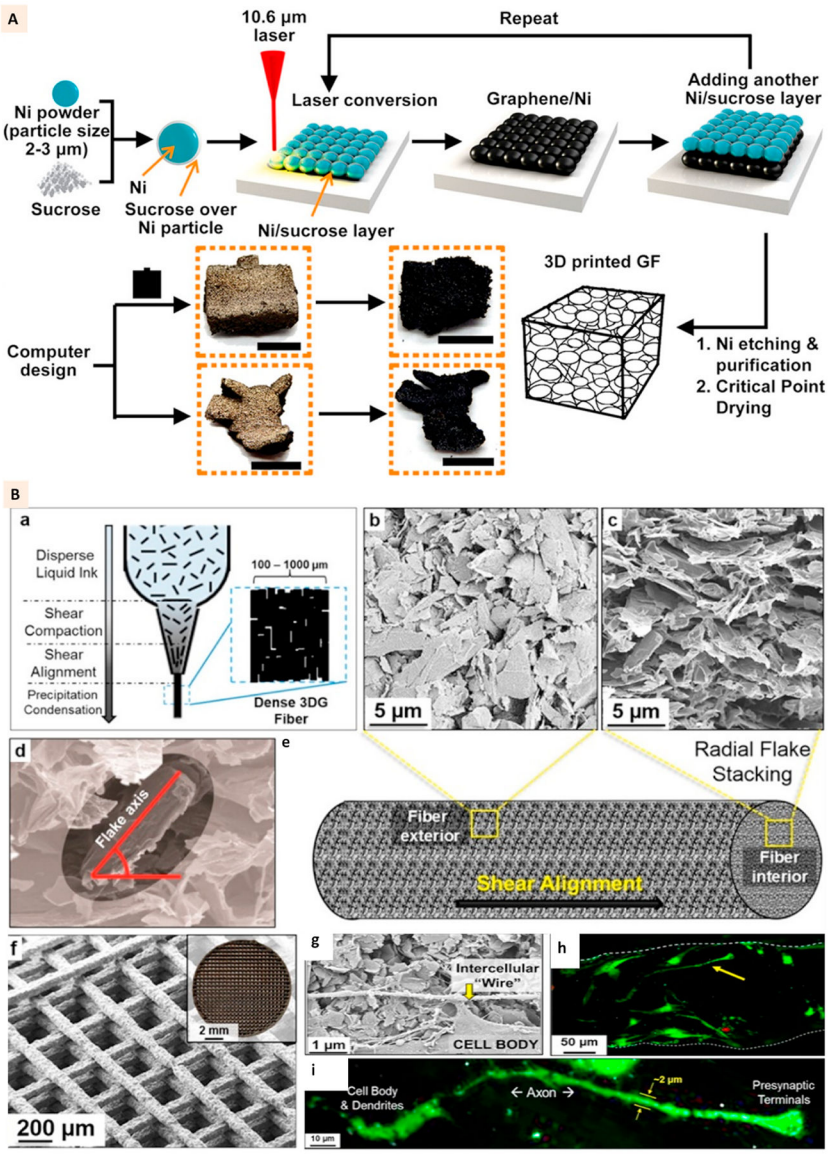

Fig. 2.

(A) Schematics showing the 3D printing of graphene foams and images of the 3D printed graphene foams before and after dissolving the nickel layer. Scale bar: 5 mm. (Adapted with permission from Ref. [30], Copyright 2017, American Chemical Society). (B) 'a' shows the liquid nature of graphene-PLG ink prior to application of pressure and flow, 'b', 'c', 'd', and 'e' show the images of graphene flake alignment along the exterior of extruded fibers and flake stacking within the fibers. 'f' shows the SEM and optical (inset) image of 3D printed structure. 'g' shows the SEM image of hMSC connecting via a small segment of long intercellular wire on the scaffolds at day 7. 'h' and 'i' show the confocal images of cells with neuronal structures growing on the scaffolds (Adapted with permission from Ref. [31], Copyright 2015, American Chemical Society).

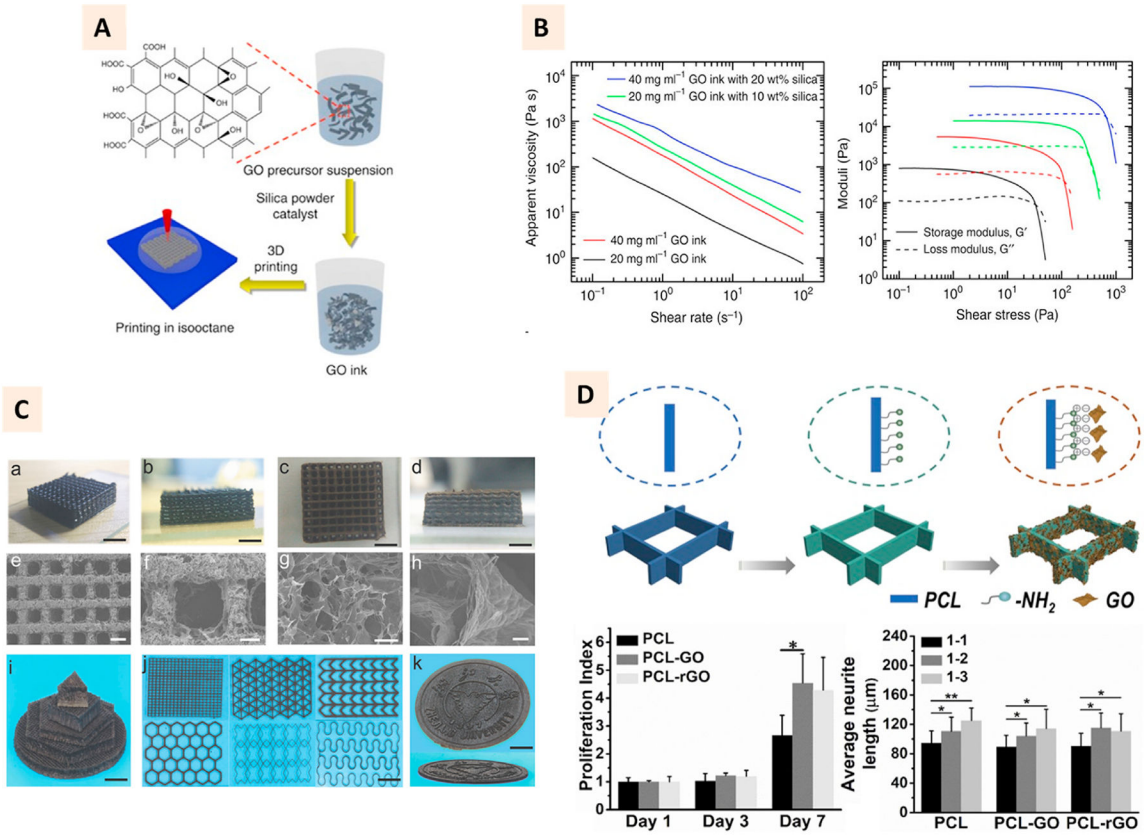

Fig. 3.

(A) Schematic demonstration of direct ink writing of GO ink to develop aerogel microlattices. The addition of silica and catalyst to GO aqueous suspension enabled direct ink writing of GO ink. (B) Charts showing the apparent viscosity vs. shear rate and shear modulus vs. shear stress of GO ink with and without silica fillers. (Adapted with permission from Ref. [33], Copyright 2021, Springer Nature). (Ca-k) Photographs and SEM images of GO microlattices printed with calcium chloride as ionic gelation agent. (Adapted with permission from Ref. [32], Copyright 2018, John Wiley and Sons). (D) Schematic showing the coating process of GO to 3D printed PCL scaffolds. Proliferation index of PC-12 cells on 1–2 anisotropic design and average neurite length on 1–1 isotropic, and 1–2 and 1–3 anisotropic designs. (Adapted with permission from Ref. [73], Copyright 2020, Elsevier).

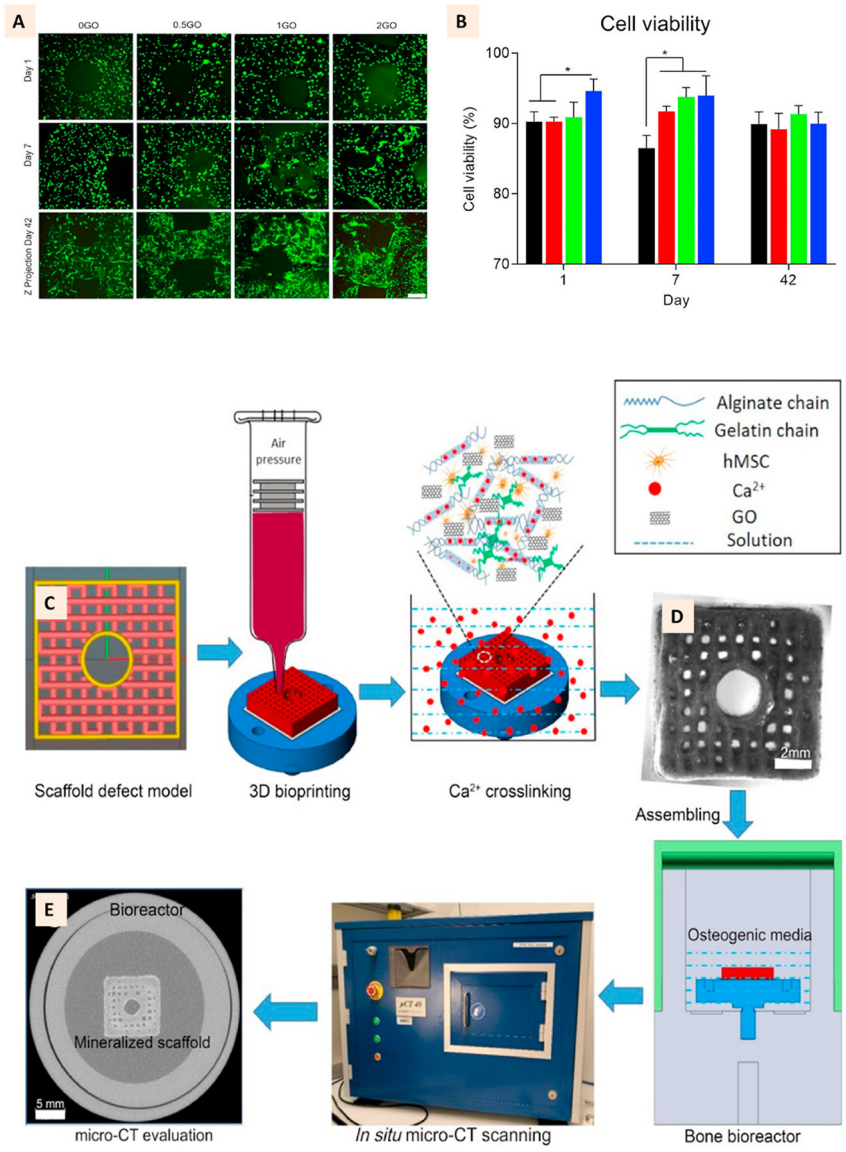

Fig. 4.

(A) Live/Dead cell-stained image showing the excellent viability of hMSC in the 3D bioprinted cell-laden GO scaffolds at day 1, 7, and 42. (B) Quantitative representation of cell viability showing GO role in improving cell viability (C) Defect scaffold STL model for bioprinting and the ink composition. (D) Representative images of the 3D cell-laden GO defect scaffold at day 1 after printing and the bioreactor setup for *in situ* micro-CT scanning. (E) 2D CT slide image after culture in osteogenic medium for 42 days showing the mineralization of construct. (Adapted with permission from Ref. [44], Copyright 2020, Elsevier).

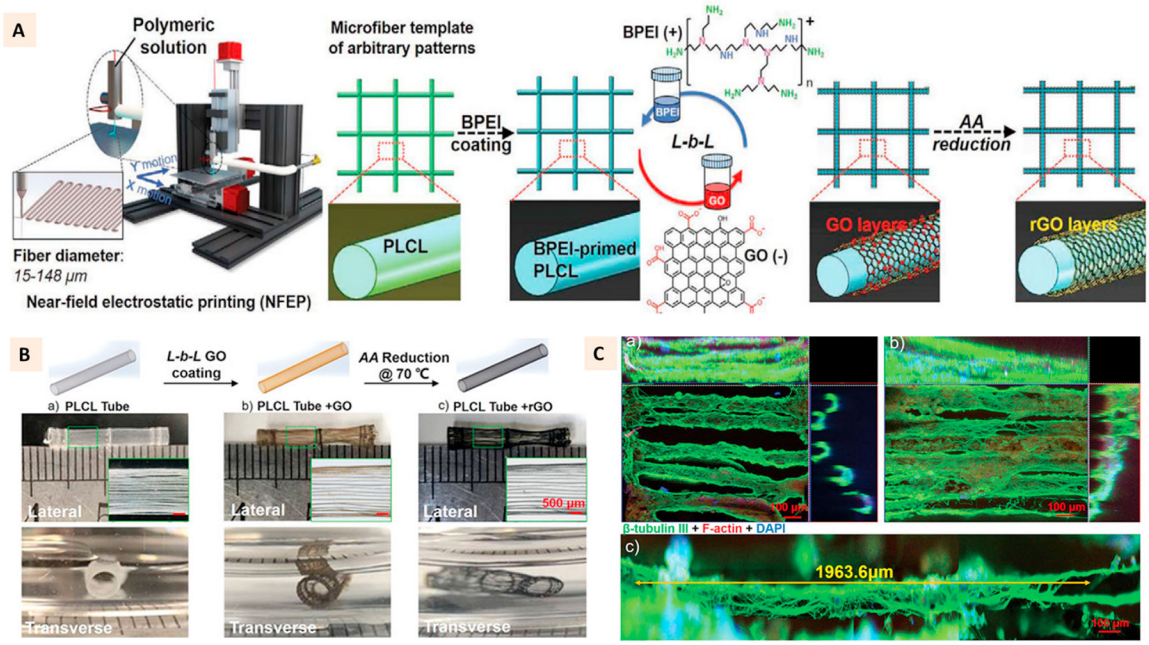

Fig. 5.

(A) Schematic illustration of the preparation of rGO encapsulated PLCL microfiber patterns using near-field electrostatic printing and layer-by-layer coating. (B) Schematics and macroscopic images of 3D tubular constructs with axially oriented GO and rGO encapsulated PLCL microfibers. (C a-c) Immunofluorescence images showing the neurite outgrowths of PC-12 cells on rGO encapsulated tubules. (Adapted with permission from Ref. [82], Copyright 2020, John Wiley and Sons).

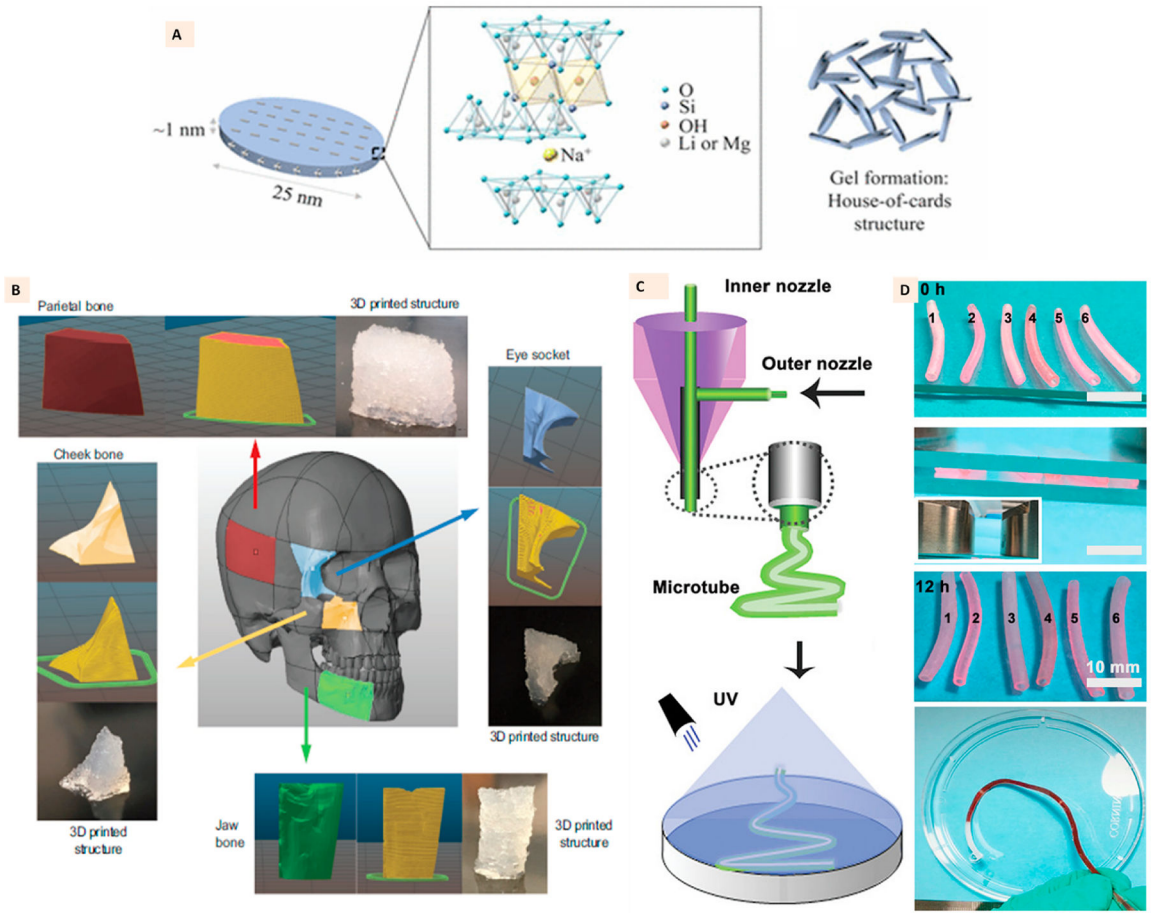

Fig. 6.

(A) Single layer of Laponite clay with its structural formula and house-of-cards arrangement of several layers in laponite gel. (Adapted with permission from Ref. [96], Copyright 2017, American Chemical Society). (B) 3D printed anatomical structures with Laponite-GelMa-kappa carrageenan ink demonstrating high printing fidelity and high design precision to reproduce the anatomical craniomaxillofacial defects. (Adapted with permission from Ref. [100], Copyright 2020, John Wiley and Sons). (C) Coaxial extrusion printing of Laponite, GelMa, and NAGA ink to develop hydrogel microtubes with high strength, perfusability, and endothelialization, (D) Photographs of printed microtubes with the demonstration of perfusion through tubes. (Adapted with permission from Ref. [103], Copyright 2020, John Wiley and Sons).

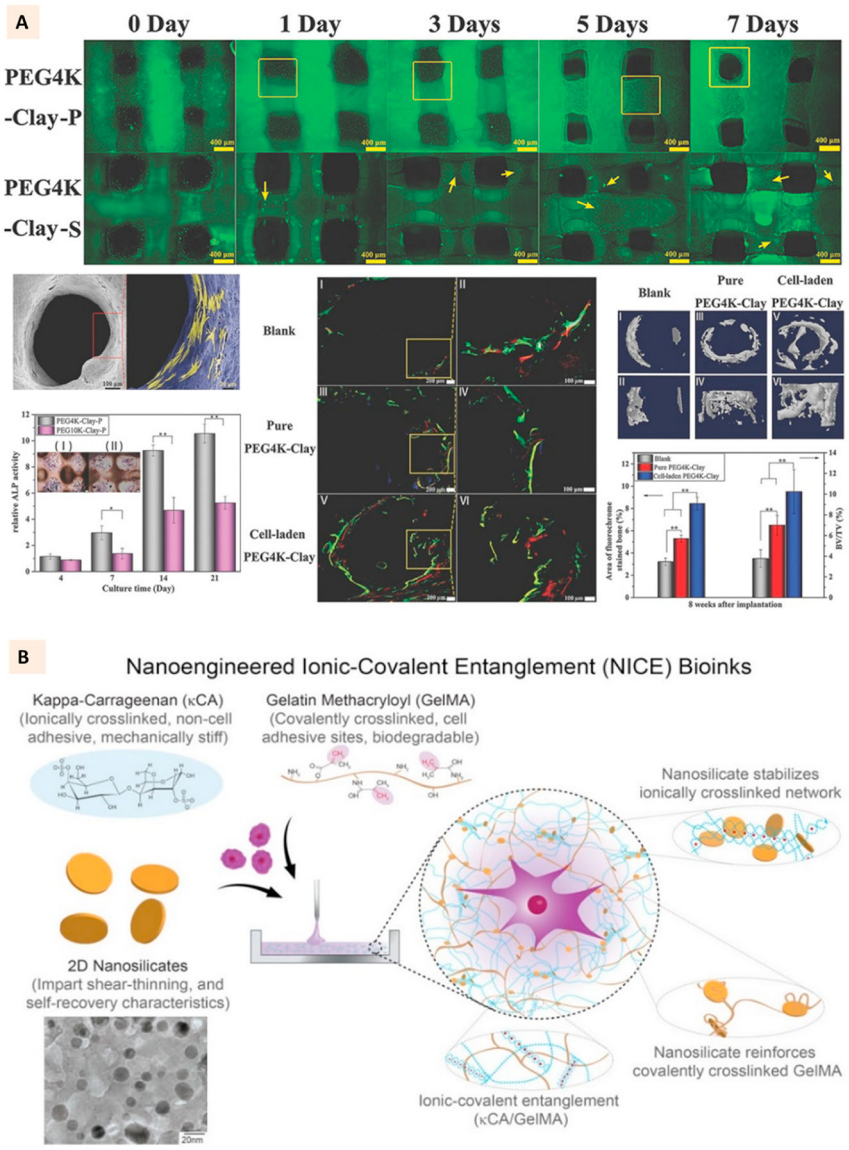

Fig. 7.

(A) Live/Dead cell assay for 3D bioprinted PEG-laponite constructs developed with two channel extrusion printing. One channel printed PEG-laponite and another channel deposited cells-hyaluronic acid laden in layer-by-layer fashion. SEM images showing the cell attachment to PEG-laponite scaffolds. Relative ALP activity and ALP stain (cross section) of PEG-laponite cell-laden constructs and the evaluation of *in vivo* bone formation with the cell-laden constructs in rat tibia model. (Adapted with permission from Ref. [108], Copyright 2017, John Wiley and Sons). (B) Constituents of NICE bioink where laponite is used to reinforce an ionic-covalent entanglement hydrogel developed with GelMa and kappa-carrageenan. TEM images show the uniform morphology of laponite particles. (Adapted with permission from Ref. [99], Copyright 2018, American Chemical Society).

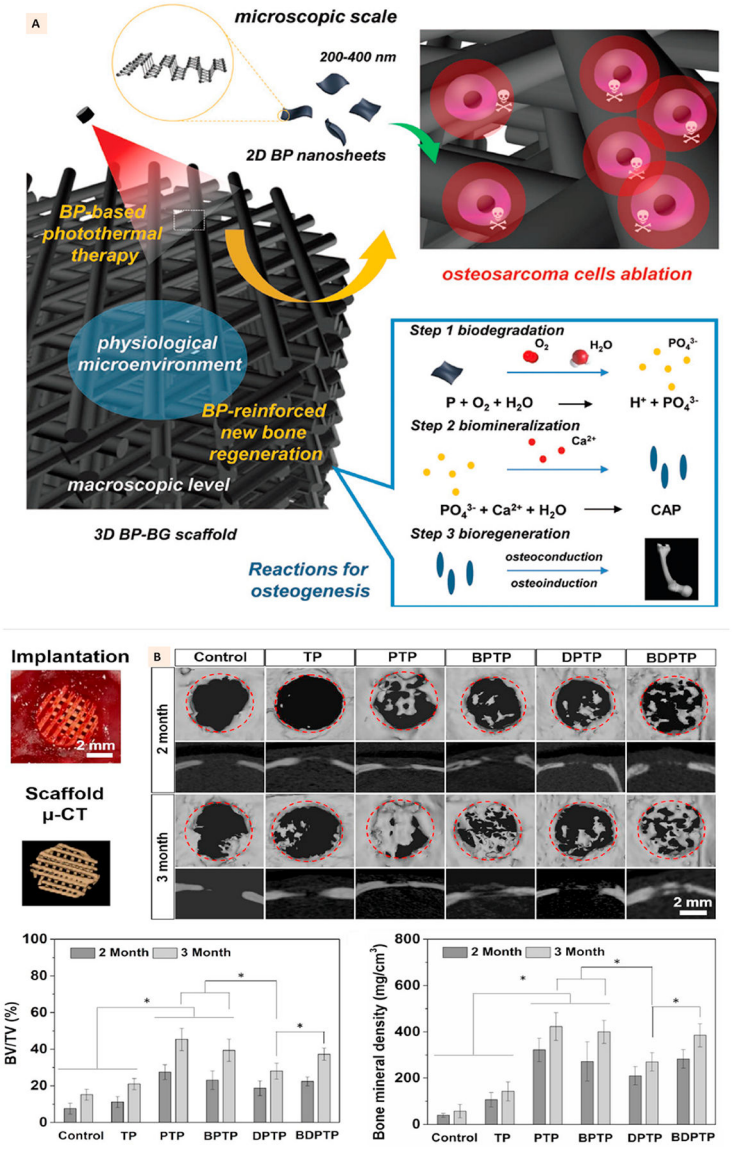

Fig. 8.

(A) Schematic illustration of fabrication of bifunctional scaffolds with black phosphorus and bioactive glass using extrusion printing and the stepwise therapeutic strategy for the removal of osteosarcoma followed by osteogenesis through BP-induced photothermal therapy and biomineralization. (Adapted with permission from Ref. [128], Copyright 2018, John Wiley and Sons). (B) *In vivo* bone regeneration in cranial defects of rats implanted with different groups of multifunctional PLGA scaffolds. The scaffolds with calcium phosphate and BP showed better bone regeneration at defect site compared to other groups. (Adapted with permission from Ref. [129], Copyright 2020, IOP Publishing Ltd).

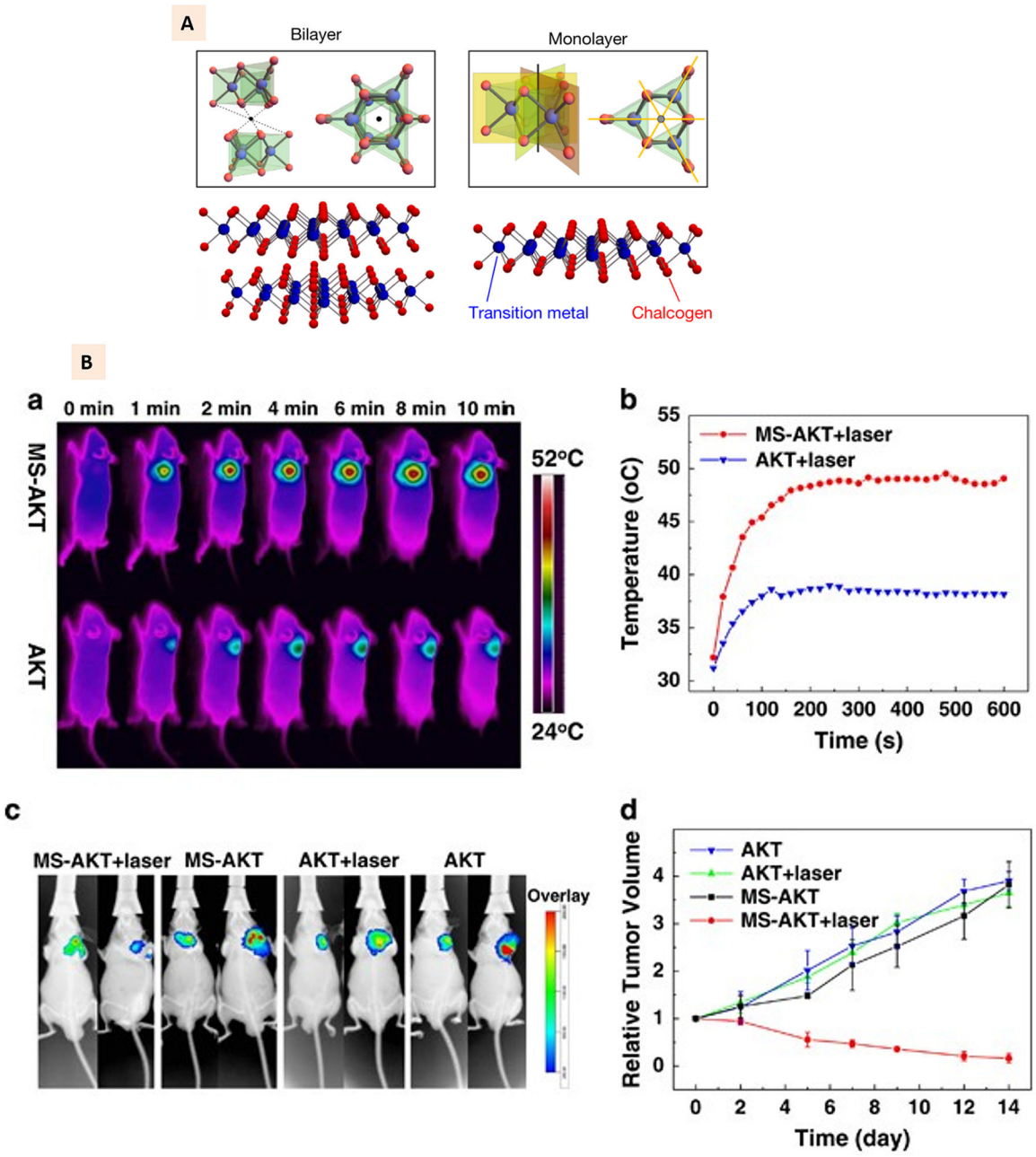

Fig. 9.

(A) Illustration of monolayer and bilayered transition metal dichalcogenides with representative atomic arrangement. (Adapted with permission from Ref. [131], Copyright 2019, Springer Nature). (B) Molybdenum disulfide-modified akermanite (MS-AKT) scaffolds implantation to mice tumor and corresponding NIR thermal images and heating curves at different time intervals. Bottom panel shows the whole-body fluorescence imaging of tumor and the quantitative analysis of relative tumor volume for different treatment groups at different time points [137], Copyright 2017, Springer Nature).

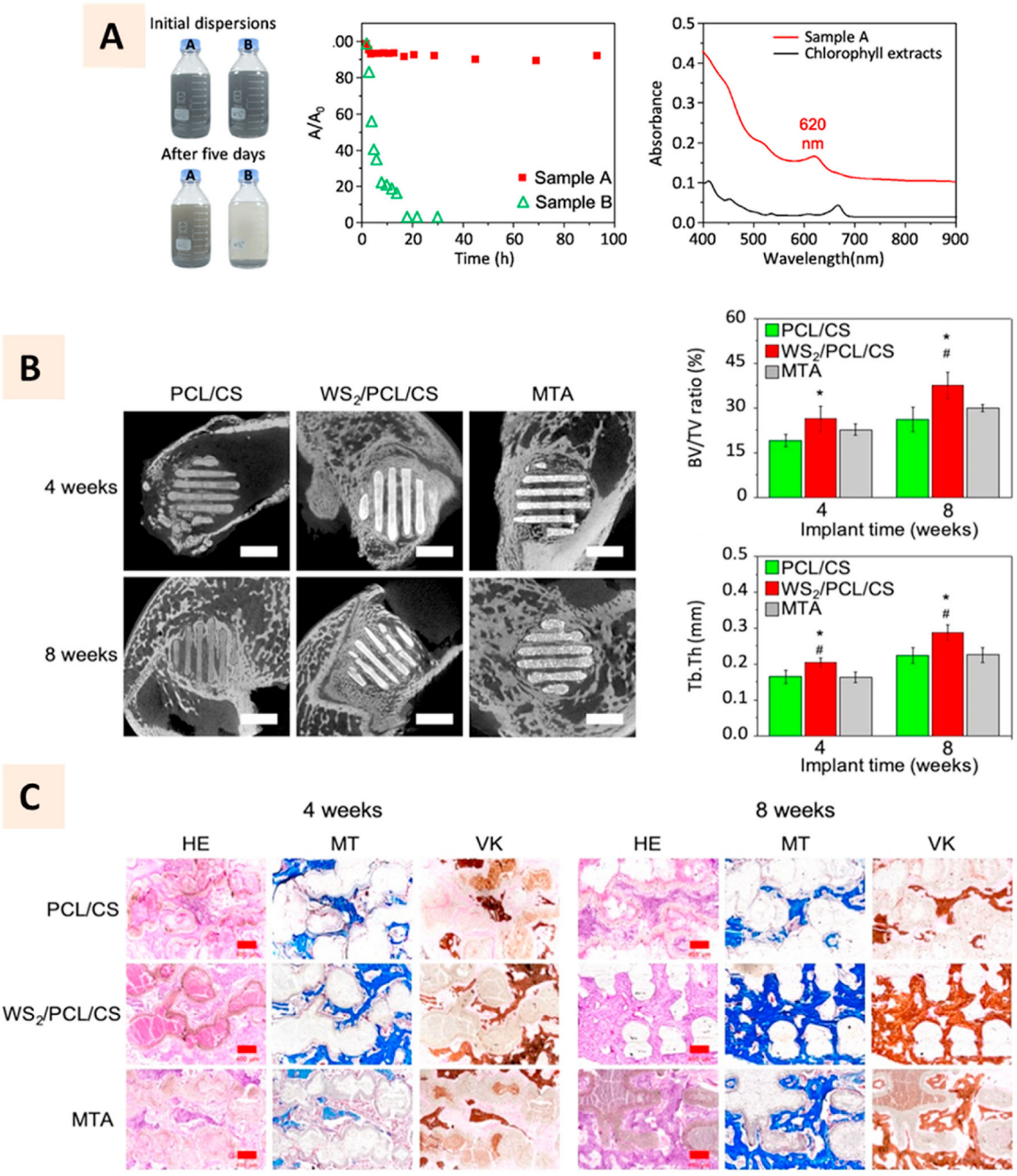

Fig. 10.

(A) Photographs showing the chlorophyll-assisted synthesis of tungsten disulfide suspension to improve its exfoliation in polymer solution. Bottle A having chlorophyll showed excellent dispersion in acetone compared to that without chlorophyll in bottle B. Absorbance ratios of the suspension shows better stability of samples with chlorophyll than without it. Characteristic absorbance of exfoliated tungsten disulfide thin sheets and extracted chlorophyll molecules. (B) Micro-CT images and qunaitifcation of bone formation at 4 and 8 weeks after implantation of PCL-tungsten disulfide to rabbit femoral defects. (C) Histology images showing the bone footnprints along the struts of 3D printed scaffolds

with more prominence observed on tungsten disulfide incorporated scaffolds (Adapted with permission from Ref. [138], Copyright 2020, Springer Nature).

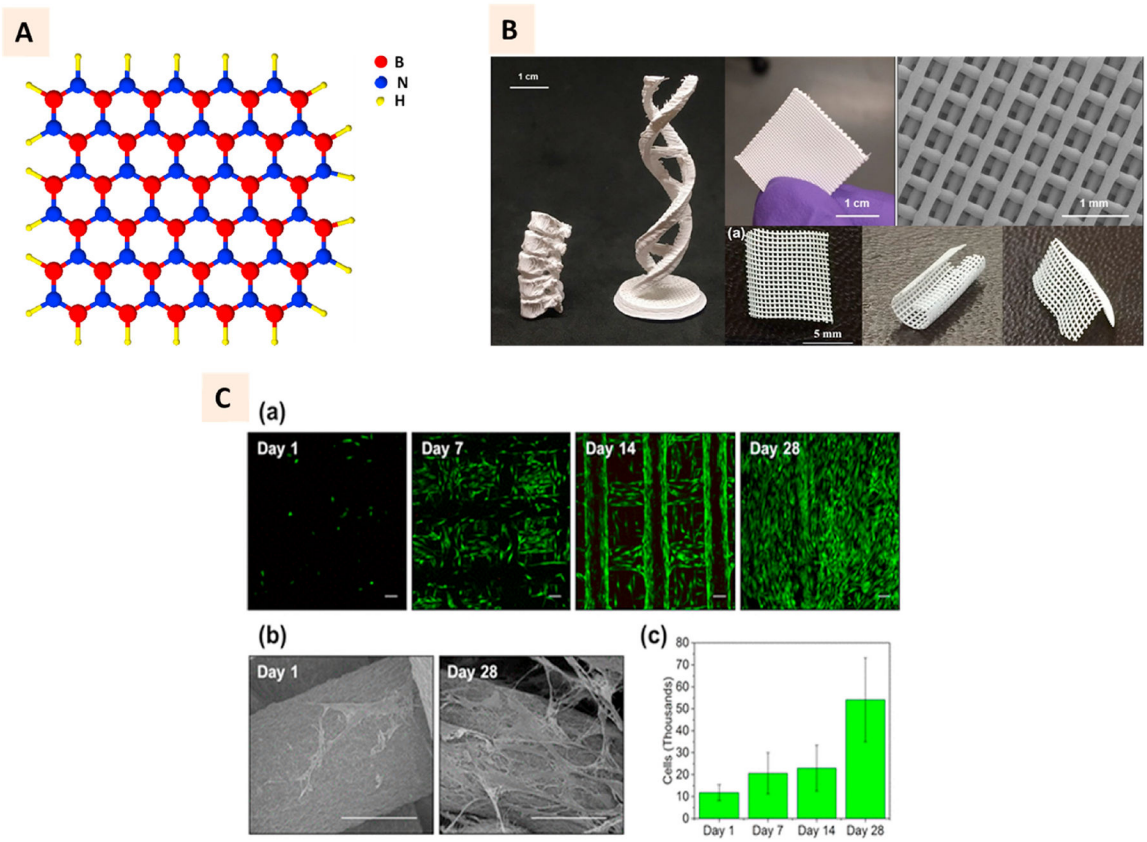

Fig. 11.

(A) 2D structure of hexagonal boron nitride (hBN) with red sphere representing boron atom, blue sphere representing nitrogen atoms, and yellow sphere representing hydrogen atom. (B) Photographs of 3D printed hBN-PLGA nanocomposites in different shapes such as lumbar spine replica, double helix, scaffold meshes and sheets. SEM image shows the individual strands of printed grids. (C) a, b Cytocompatibility of composite scaffolds illustrated with live/dead cell assay showing the attachment of viable hMSC at different days of culture and SEM images showing the spreading of cells. c Quantitative DNA assessment showing the proliferation of cells on the composite scaffolds over 4-week period. (Adapted with permission from Ref. [161], Copyright 2018, American Chemical Society).

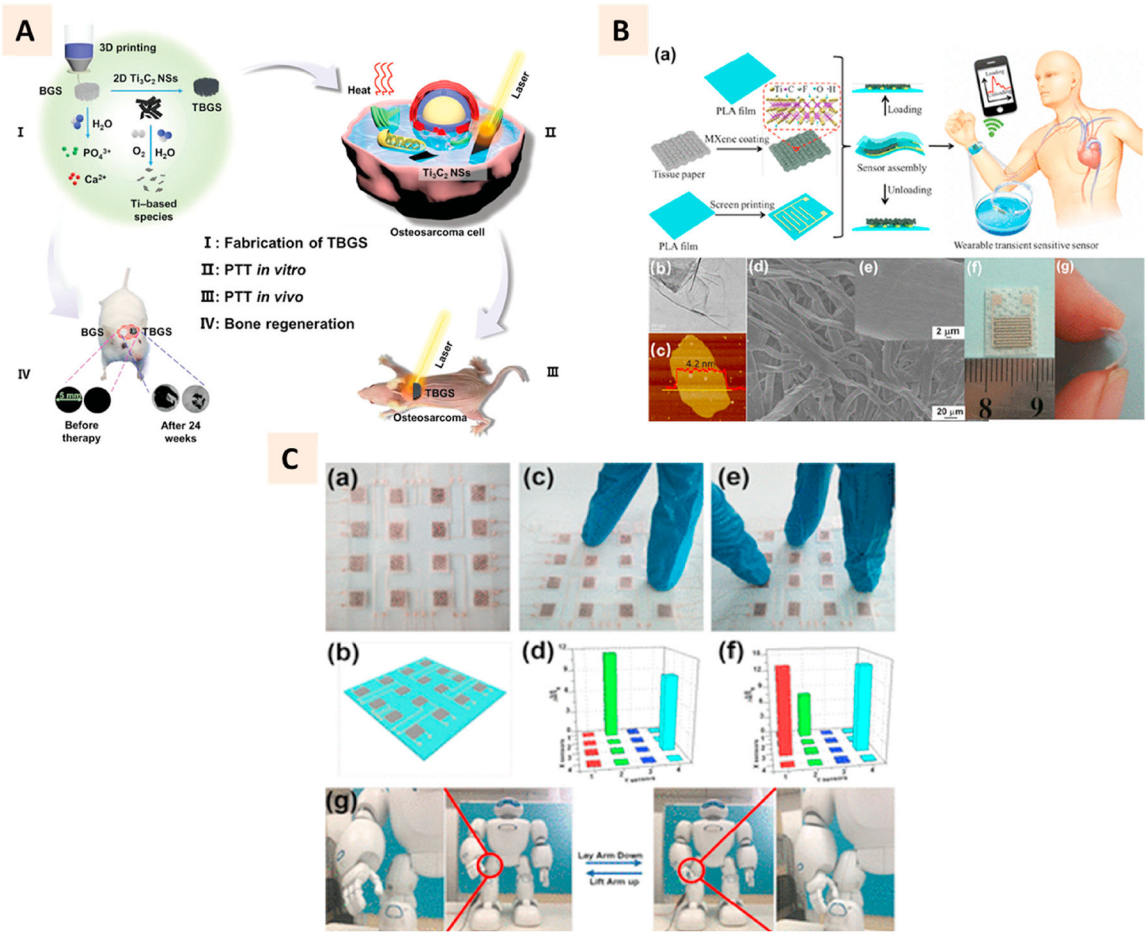

Fig. 12.

(A) Schematic illustration of Ti_3C_2 MXene and bioactive glass (TBGS) scaffold fabrication using 3D printing and their application in bone tumor ablation, and bone tissue regeneration in four steps. (Adapted with permission from Ref. [171], Copyright 2019, John Wiley and Sons). (B) a Schematics of the fabrication process of flexible wearable transition pressure sensors with MXene nanosheets using screen printing technique. b-e TEM, AFM, and SEM characterization of Mxene nanosheets. f-g Photographs of the flexible wearable transient pressure sensor. (C) a-b Photograph of pressure sensor built from MXene and its schematic. c-f Application of two and three fingers on the pressure sensors and corresponding pressure distribution mapping from the sensing responses. g Attachment of pressure sensor to a robot femorotibial joint to measure the sensing responses remotely. (Adapted with permission from Ref. [178], Copyright 2019, American Chemical Society).

Table 1

Studies focusing on local and systemic toxicity of pure 2D materials.

Type of material	Treatment type	Cell type/Animal model	Effect	Reference
Graphene nanoplatelets (GNPs)	*In vitro*	Human bronchial epithelial cell line (BEAS-2B)	Dose-dependently reduced cell viability, which was accompanied by an increase in the portion of cells in the subG1 and S phases, downregulated the generation of ROS, suppressed ATP production, damaged mitochondria, and elevated levels of autophagy-related proteins	[181]
	In vivo	Mice	Subchronic inflammatory response	
Graphene quantum dots (GQDs)	*In vitro*	Cancer cell lines (KB, MDA-MB231, A549) Normal cell line (MDCK)	No acute toxicity or morphological changes	[182]
Graphene quantum dots (GQDs)	*In vivo*	Mice	GQDs mainly accumulated in liver, spleen, lung, kidney, and tumor sites after intravenous injection.	
			No toxicity to the treated animals or organ damage/lesions to treated mice after 21 days of administration at 5 mg/kg or 10 mg/kg dosages	
	In vitro	HeLa (A549) cells	Low cytotoxicity	[212]
	In vivo	Mice	No material accumulation in main organs and fast clearance of GQDs through kidney	
GO and rGO	*In vitro*	HEK 293T cells	Small and large sizes of G and GO significantly reduced the cell viability and increased DNA damage, accompanying with activated reactive oxygen species (ROS) generation and induced various expressions of associated critical genetic markers	[183]
	In vivo	Zebrafish	G showed stronger ability to decrease the survival rate and induce the acute toxicity, while GO showed obvious toxicity in terms of DNA damages, ROS generation, and abnormal gene expressions	
	In vitro	Luminous Tox2 & RecA bacterial strains	G and GO caused strong acute toxicity on Tox2 bacteria; G was more toxic than GO and showed size dependent effect with toxicity increasing with increase in size. GO induced mild genetic toxicity on RecA bacteria	
	In vitro	Murine macrophage RAW 264.7 cells	ROS-mediated toxic effects with pristine graphene	[184]
	In vitro	*E. coli*; *S. aureus*	Bacteria cell membrane damage: GO at a concentration of 85 μg/ml could suppress the growth of *E. coli* after 2 h incubation at 37 °C	[185]
	In vivo	Mice	Chronic toxicity with high dose (0.4 mg) in lung, liver, spleen, kidney	[189]
	In vitro	*E. coli, Pseudomonas aeruginosa*	No noticeable antimicrobial effect with GO alone	[187]
	In vivo	Mice	Accumulates in reticuloendothelial system (RES) organs, such as liver and spleen at early time points after IV injection	[213]
	In vitro	Human platelets	Evokes aggregatory response, which may play a role in hemostasis and thrombus formation	[180]
	In vivo	Mice	Thrombogenic	
	In vitro	HeLa cells	Dose-dependent toxicity	[184]
	In vivo	Zebrafish	Polyacrylic acid (PAA) was used to functionalize GO to reduce its toxicity to cells	
	In vitro	A549 human epithelial cells	GO does not enter A549 cell and has no obvious cytotoxicity, but can cause a dose-dependent oxidative stress in cell and induce a slight loss of cell viability at high concentration	[214]

Type of material	Treatment type	Cell type/Animal model	Effect	Reference
	In vivo	Mice	Induce the mitochondrial generation of ROS, activate inflammatory and apoptotic pathways, and result in severe and persistent lung injury	[184]
	In vitro	U87 and U118 glioma cell lines	Both types of platelets reduced cell viability and proliferation with increasing doses, but rGO was more toxic than GO with rGO increasing the level of apoptotic markers in treated tumors	[215]
	In vivo	Mice	Short-term repeated GO exposure can cause obvious intraocular inflammation, an incrassated corneal stromal layer, cell apoptosis in the cornea, iris neovascularization and significant cytotoxicity of rat corneal epithelial cells (rCECs), while RGO causes no significant ocular toxicity in mice	[190]
Laponite® XLG, nanohybrids	*In vitro*	Cancer cells (KB human epithelial carcinoma cells, MCF-breast cancer cells, CAL-72 osteosarcoma cell lines)	Cytotoxicity towards cancer cells	[216]
	In vivo	Mice	Absence of organ toxicity 24 h and half a month post IV injection	
	In vitro	Human mesenchymal stem cells (hMSCs)	Non-toxic at concentrations less than 1 mg/ml	[192]
	In vivo	Rats	Implantation of Laponite bioceramics does not show acute systemic toxicity or irritation to normal skin of rats	[193]
MMT	*In vitro*	INT-407 (intestinal) cells	MMT could cause cytotoxic effects in a concentration- and time-dependent manner and at high concentration after long-time exposure	[195]
	In vivo	Mice	MMT absorbed within 2 h but did not accumulate in any specific organ or showed any remarkable toxicity	
	In vitro	HUVE, N1E-115 and ROC-1 cell lines	Decrease cell viability in HUVECs exposed for 24 h to 0.1 mg/ml but limited results in neuronal cell lines N1E-115 and ROC-1	[217]
	In vitro	CHO cells	Reduction in cell viability after being exposed to 1 mg/ml for up to 24 h	
MMT nanocomposite (MMN)	*In vivo*	Broiler chicks	Addition of 3 g MMN/kg AF-contaminated diet diminished the adverse effects of AF on most relative organ weights, hematological values, serum and liver biochemical values and enzymatic activities associated with aflatoxicosis in broiler chicks	[218]
BP nanosheets	*In vitro*	Human bronchial epithelial cells	BP nanosheets decrease viability of these cells in a time- and dose-dependent manner via interference with mitochondrial membrane potential, leading to an increase in intracellular ROS, activation of caspase-3, and apoptosis	[219]
	In vivo	Mice	Single injection of BP nanosheets does not cause toxicity in a short period of time, whereas multiple injections of BP nanosheets exert adverse effects on liver and renal function	
BP quantum dots (BPQDs)	*In vitro*	HeLa cells	At high concentration (200 μg/ml) exhibit significant apoptotic effects	[211]
	In vivo	Mice	BPQD can transiently induce oxidative stress, including lipid peroxidation, reduction of catalase activity, DNA breaks, and bone marrow nucleated cells (BMNC) damage, but recovered gradually to healthy levels and no pathological damage to organs is apparent	
Black phosphorus (BP)-quantum dots (QDs)	*In vitro*	Kidney organoid	Moderate toxicity	[209]
	In vitro	Huma renal tubular epithelial cells	Nephrotoxicity	
	In vivo	Mice	Nephrotoxicity - found to cause insulin insensitivity and endoplasmic reticulum strees in the kidney	

Type of material	Treatment type	Cell type/Animal model	Effect	Reference
MoS_2, WS_2, and WSe_2	*In vitro*	Lung epithelial carcinoma cells	WS2 elicit slightly more toxic responses whereas MoS2 and WS2 are safe and less hazardous	[199]
MoS_2 nanosheets	*In vitro*	NIH-3T3 murine embryo fibroblast cells and the human adipose derived mesenchymal stem cells	Mild toxicity	[220]
		Human embryonic lung fibroblast (HELF) cells	Bovine serum albumin (BSA) coating diminished the toxic effect, and both coated and uncoated NPs promoted the proliferation of HELF cells, which, as a pathological process, can lead to idiopathic pulmonary fibrosis	
	In vitro	HepG2 cells	Cell membrane disruption: ROS level and the mitochondrial membrane potential were altered in the treated cells, suggesting oxidative stress and apoptosis induction; inhibition of ABC transporter	
	In vitro	BEAS-2B immortalized human bronchial epithelial cells; THP-1 human monocytic cells	Cell viability unaltered with proinflammatory effect for aggregates and low effect for nanoforms	
	In vivo	Mice	Proinflammatory effect for aggregates and low effect for nanoforms	
MoS_2 nanofilm and microparticles	*In vitro*	PANC1 human pancreatic cancer cells; 293 human embryonic kidney cells; human pancreatic duct epithelial (HPDE) cells; human mammary epithelial (HMLE) cells; SUM159 mesenchymal triple-negative breast cancer cells; MDAMB-231 invasive ductal breast carcinoma cells	Cell viability unaltered up to 0.016 mg/ml, slight decrease in viability for higher concentrations	
	In vivo	Guinea pigs	No skin allergy symptoms	
Molybdenum trioxide (MoO_3) nanoparticles	*In vitro*	Human MCF-7 (breast cancer) and HepG2 (hepatoma)	Showed a dose-dependent decrease in viability at concentrations (25–0.625 μg/ml)	
		C18–4 spermatogonial stem cell line	Cell membrane integrity disruption	
		BRL 3A cells (immortalized rat liver cells)	Mildly toxic effect at 250 μg/ml but significant LDH leakage present at the concentration of ≥100 μg/ml.	
MoO_2 and MoO_3 nanocolloids	*In vitro*	NIH/3T3 cell line	Decreased viability in a concentration dependent manner associated with a change in the redox status of the cell, resulting in oxidative stress induction	
MoO_3 nanoplates	*In vitro*	Human breast cancer cells (MCF-7 and the invasive type MCF-7 with the CD44high/CD24low phenotype) and human keratinocyte (HaCaT)	HaCaT cells did not show decreased viability, but both MCF-7 lines were susceptible and likely to involve the loss of the mitochondrial membrane potential and an induction of oxidative stress	
hBN nanosheets	*In vitro*	*E. coli* DH5α	Degradation of bacterial cell membranes (inner and outer layers)	[201]
hBN nanoparticles	*In vivo*	Rats	Damage in the liver, kidney, heart, spleen, and pancreas at 1600 and 3200 μg/kg doses	[205]
hBN nanosheets and nanoparticles	*In vitro*	Osteoblast-like cells (SaOS2)	Decrease in cell viability in presence of both nanosheets and nanoparticles with the smallest size likely attributed to internalization and activation of ROS	[205]
hBN flakes	*In vitro*	Mouse hippocampal cell line (mHippo E14)	No cytotoxic effects at hBN concentration lower than 22 μg/ml and favored the cell survival after exposure to doxorubicin	

Type of material	Treatment type	Cell type/Animal model	Effect	Reference
Ti_3C_2 and Nb_2C Mxene quantum dots	*In vitro*	Human umbilical vein endothelia cells (HUVECs)	Ti_3C_2 QDs could induce cytotoxicity to HUVECs at 100 μg/ml	[221]
MXene flake/Cu nanocomposite	*In vitro*	3T3 mouse fibroblasts and HEK293 cells	No toxic effects	[222]
Ti_3C_2Tx MXene film	*In vitro*	Mouse pre-osteoblast cell line MC3T3E1	No cytotoxicity	[207]
	In vivo	Rat calvaria	No toxic or inflammatory effects; improves osteogenesis	
	In vivo	Mice	No adverse effects or pathological toxicity (20 mg/kg)	
MXene, Nb_2C-PVP nanosheets				[222, 223]
MXene nanosheets	*In vivo*	Avian embryos	Adverse effect on the early stage of embryogenesis as ~46% of MXene-exposed embryos died during 1–5 days after exposure and may inhibit angiogenesis of the chorioallantoic membrane of the embryo after 5 days of incubation; seven genes that are key regulators of cell proliferation, survival, cell death and angiogenesis were deregulated in brain, heart, and liver tissues	[224]
	In vivo	Zebra fish embryos	LC50 of Ti3C2Tx was greater than 100 μg/ml, it can be classified as within the “practically nontoxic” group according to the Acute Toxicity Rating Scale by the Fish and Wildlife Service (FWS)	[225]